Journal of Geophysical Research: Atmospheres

RESEARCH ARTICLE

Key Points:
- Decadal and interannual variations of BC in China were systematically analyzed for 1980–2010
- Decadal trends of BC were mainly dependent on variations of emissions
- Interannual variations of BC were driven by changes in meteorological parameters and emissions

Correspondence to:
Y.-H. Mao,
yhmao@mail.iap.ac.cn

Impacts of meteorological parameters and emissions on decadal and interannual variations of black carbon in China for 1980–2010

Yu-Hao Mao[1], Hong Liao[1], Yongming Han[2,3], and Junji Cao[3]

[1]State Key Laboratory of Atmospheric Boundary Layer Physics and Atmospheric Chemistry, Institute of Atmospheric Physics, Chinese Academy of Sciences, Beijing, China, [2]Key Laboratory of Atmospheric Chemistry and Physics, Institute of Earth Environment, Chinese Academy of Sciences, Xi'an, China, [3]State Key Laboratory of Loess and Quaternary Geology, Institute of Earth Environment, Chinese Academy of Sciences, Xi'an, China

Abstract We quantified the impacts of variations in meteorological parameters and emissions on decadal trends and interannual variations of black carbon (BC) in China for 1980–2010 using a global chemical transport model (GEOS-Chem) driven by the Modern Era Retrospective-analysis for Research and Applications meteorological fields. Model results reasonably captured the decadal and interannual variations of observed BC in China. From 1980 to 2010, simulated surface concentrations and tropospheric column burdens of BC increased by $0.21\,\mu g\,m^{-3}$ (29%) and by $0.29\,mg\,m^{-2}$ (37%), respectively, averaged over China; the corresponding all-sky direct radiative forcing at the top of the atmosphere increased by $0.35\,W\,m^{-2}$ (51%). Considering variations in both meteorological parameters and emissions for 1980–2010, simulated annual mean surface concentrations (column burdens) of BC were in the range of 0.7–$1.0\,\mu g\,m^{-3}$ (0.8–$1.1\,mg\,m^{-2}$) averaged over China. The associated decadal trends were $0.31\,\mu g\,m^{-3}\,decade^{-1}$ ($0.29\,mg\,m^{-2}\,decade^{-1}$) in the 1980s, -0.20 (-0.10) in the 1990s, and 0.16 (0.21) in the 2000s. The interannual variations were -20% to 15% (-20% to 11%) for deviation from the mean, $0.068\,\mu g\,m^{-3}$ ($0.069\,mg\,m^{-2}$) for mean absolute deviation, and 7.7% (7.1%) for absolute percent departure from the mean. Model sensitivity simulations indicated that the decadal trends of surface concentrations and column burdens of BC were mainly driven by changes in emissions, while the interannual variations were dependent on variations of both meteorological parameters and emissions.

1. Introduction

Black carbon, as an important component of atmospheric particulate matter (PM), affects both air quality and climate [*Bond et al.*, 2013; *Intergovernmental Panel on Climate Change* (*IPCC*), 2013]. Black carbon has substantial impacts on climate because of its strong absorption of solar radiation [e.g., *Horvath*, 1993; *Ramanathan and Carmichael*, 2008], important influences in cloud processes [*Jacobson*, 2006], and significant impacts on snow and ice albedos [*Flanner et al.*, 2007, 2009]. China is the largest black carbon emitter in the world, contributing about 25% of the global total emissions [*Cooke et al.*, 1999; *Bond et al.*, 2004; *Wang et al.*, 2012; *Qin and Xie*, 2012]. Black carbon (BC) emissions in China have dramatically increased from 1980 because of the large energy consumption. The growth rate of BC emissions in China was ~38% between 1980 and 1990 [*Ohara et al.*, 2007] and ~46% between 2000 and 2010 [*Lu et al.*, 2011]. Because of the high emissions, annual mean surface BC concentrations are typically in the range of 2–$5\,\mu g\,m^{-3}$ at rural sites [*Zhang et al.*, 2008] and annual direct radiative forcing (DRF) due to BC is 0.58–$1.46\,W\,m^{-2}$ at the top of the atmosphere (TOA) averaged over China (summarized in *Li et al.*, [2016]). Because of its shorter lifetime relative to long-lived greenhouse gases, BC reduction may provide an efficient near-term solution to mitigate global warming and to improve air quality and public health simultaneously [*Ramanathan and Carmichael*, 2008; *Shindell et al.*, 2012; *Bond et al.*, 2013; *Smith and Mizrahi*, 2013]. Note that there are large uncertainties in net climate effect of black carbon-rich sources and therefore in the response to mitigation, as BC is coemitted with many species (e.g., organic matter and sulfate) that have a cooling effect and counter the global warming effect of BC [e.g., *Penner et al.*, 2010; *Bond et al.*, 2013].

Quantifying the decadal and interannual variations of BC and understanding the drivers of the variations are critical for guiding BC reduction measures. A major obstacle in understanding the decadal and interannual variations of BC in China is the lack of a consistent and long-term measurement network in China with good

spatiotemporal coverage, such as the Interagency Monitoring of PROtected Visual Environment (IMPROVE) network in the United States [*Malm et al.*, 1994]. In the past decade, many studies have measured BC concentrations at Chinese urban and rural sites [e.g., *Zhang et al.*, 2008, 2012]. However, most of such measurements were conducted at a few locations for short periods. Historical BC in ice cores [e.g., *Ming et al.*, 2008; *Xu et al.*, 2009], lake sediments [e.g., *Han et al.*, 2011; *Cong et al.*, 2013], and peat lands [e.g., *Gao et al.*, 2014] has been reconstructed in China in recent years. These valuable data are an ideal mean to examine the long-term variation of BC back to the preindustrial times.

The decadal and interannual variations of BC are influenced by both emissions and meteorology. Meteorological parameters influence BC concentrations through altering emissions (biomass burning), transport, and deposition. Modeling studies by *Mu and Liao* [2014] showed that variations in meteorological fields dominate the interannual variations of aerosols in China over 2004–2012. *Yang et al.* [2015] reported that the decadal trends and interannual variations of outflow fluxes of aerosols from East Asia for 1986–2006 are mainly driven by variations in emissions and meteorological parameters, respectively. *M. Wang et al.* [2014] showed that the overall increasing trend in deposition fluxes of BC at the Zuoqiupu glacier since 1980 is consistent with the increasing BC emissions in South Asia. *Jeong and Park* [2013] argued that meteorological conditions account for an increase of winter PM in East Asia by 7% over the past two decades.

Modeling studies can provide a useful tool for better understanding of the change of BC in China on a decadal time scale. To our knowledge, few studies have systematically examined the decadal and interannual changes of aerosols in China and analyzed their driving factors. Even fewer studies focused on BC due to the lack of observations and the limitation of models. Here we present the decadal trends and interannual variations of surface concentrations and tropospheric column burdens of BC in China for a 31 year period (1980–2010) using a global chemical transport model (GEOS-Chem) driven by the Modern Era Retrospective-analysis for Research and Applications (MERRA) meteorological fields. We aim to quantify the roles of variations in meteorological parameters, anthropogenic and biomass burning emissions in the decadal trends, and interannual variations of BC in China. We describe the GEOS-Chem model, numerical simulations, and observations for model evaluation in section 2. The evaluations of GEOS-Chem are discussed in section 3. In sections 4 and 5, we present the impacts of variations in emissions and meteorological parameters on the decadal trends and interannual variations of BC. Changes in all-sky TOA DRF of BC are discussed in section 6. Finally, summary and conclusions are given in section 7.

2. Methods

2.1. GEOS-Chem Model

2.1.1. Model Description

The GEOS-Chem model is driven by assimilated meteorology from the Goddard Earth Observing System (GEOS) of the NASA Global Modeling and Assimilation Office [*Bey et al.*, 2001]. Here we use GEOS-Chem version 9-01-03 (available at http://geos-chem.org) driven by the MERRA assimilated data for a 31 year period (1980–2010) [*Rienecker et al.*, 2011]. The native resolution of the MERRA variables is 0.5° (latitude) × 0.667° (longitude) and 72 vertical layers, and a temporal resolution of 6 h (3 h for surface variables and mixing depths). The spatial resolution is degraded to 2° (latitude) × 2.5° (longitude) in the horizontal and 47 layers in the vertical (from the surface to 0.01 hPa) for computational expediency.

Tracer advection is computed using a flux-form semi-Lagrangian method [*Lin and Rood*, 1996] every 15 min. Tracer moist convection follows *Allen et al.* [1996a, 1996b] including GEOS convective, entrainment, and detrainment mass fluxes. The deep convection in MERRA is parameterized using the relaxed Arakawa-Schubert scheme [*Arakawa and Schubert*, 1974; *Moorthi and Suarez*, 1992], and the shallow convection treatment follows *Hack* [1994]. Simulation of aerosol wet deposition is computed as described by *Liu et al.* [2001] and updated by *Wang et al.* [2011]. Wet deposition includes contributions from scavenging in convective updrafts, rainout from convective anvils, and rainout and washout from large-scale precipitation. Dry deposition of aerosols uses a resistance-in-series model [*Walcek et al.*, 1986] dependent on local surface type and meteorological conditions.

The GEOS-Chem simulation of carbonaceous aerosols has been reported previously by *Park et al.* [2003]. Eighty percent of BC emitted from primary sources is assumed to be hydrophobic, and hydrophobic aerosols
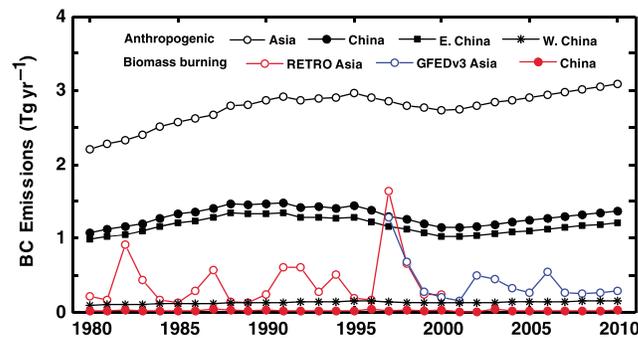
Figure 1. Annual anthropogenic (black) and biomass burning emissions (red and blue) of BC (Tg yr^{-1}) for 1980–2010 in Asia (10°S–55°N, 60°E–150°E) and China (defined by the national borders of China). Anthropogenic emissions are from REAS [*Ohara et al.*, 2007]; biomass burning emissions are from RETRO for 1980–1996 [*Schultz et al.*, 2008] and from GFEDv3 for 1997–2010 [*van der Werf et al.*, 2010]. Also shown are annual anthropogenic emissions in eastern China (east of 105°E) and western China (west of 105°E).

become hydrophilic with an *e*-folding time of 1.15 days [*Cooke et al.*, 1999; *Chin et al.*, 2002; *Park et al.*, 2003]. BC in the model is assumed to be externally mixed with other aerosol species.

The BC DRF in the present study is calculated using the Rapid Radiative Transfer Model for GCMs (RRTMG), which has been coupled online with the GEOS-Chem model [*Heald et al.*, 2014]. The RRTMG calculates cloud optical properties based on the liquid and ice visible optical depths from the MERRA meteorology. The surface albedo and emissivity (spectrally resolved) are climatology data calculated from the multiwavelength 8 day land composites of Moderate Resolution Imaging Spectroradiometer from 2002 to 2007. The RRTMG is applied to 14 shortwave bands and 16 longwave bands ranging from 0.23 to 56 μm, which ensure the accuracy in solving the radiative transfer equation. We calculate instantaneous shortwave and longwave radiative fluxes every 3 h. We assume that dry BC particles are spherical with a refractive index of 1.75–0.44*i* at 550 nm and a density of 1 g cm^{-3}, following *Q. Wang et al.* [2014]. The mass absorption coefficient (MAC) for BC is 7.5 m^2 g^{-1} at 550 nm based on observations [*Clarke et al.*, 2004]. Studies have shown that uncertainties in BC MAC range from 3 to 25 m^2 g^{-1}, depending on atmospheric conditions [*Bond and Bergstrom*, 2006].

2.1.2. Emissions

The global anthropogenic emissions of BC are from *Bond et al.* [2007] for 1980, 1990, and 2000, and emissions for year 2010 are calculated based on emissions for year 2000 by applying regional-scale factors from *Streets et al.* [2004]. Interannual variations in anthropogenic emissions are represented by annual scaling factors derived using a linear interpolation approach. We update the annual BC emissions in Asia for 1980–2010 with the Regional Emission inventory in Asia (REAS) [*Ohara et al.*, 2007, available at http://www.jamstec.go.jp/frsgc/research/d4/emission.htm]. The REAS inventory has historical emissions for 1980–2003 and predicted emissions for 2004–2010. Seasonal variations of anthropogenic emissions are considered in China and India using monthly scaling factors taken from *Kurokawa et al.* [2013]. Figure 1 shows the annual BC emissions for 1980–2010 in Asia (10°S–55°N, 60°E–150°E), China (defined by the national borders of China), eastern China (east of 105°E), and western China (west of 105°E). Relative to 1980, the Asian anthropogenic emissions in 2010 increase by 40% and the increasing rate is 0.28 Tg C decade^{-1} averaged over the period of 1980–2010. Anthropogenic emissions in Asia and China are generally increasing from 1980, except during the period of 1992–2000. Anthropogenic emissions are nearly constant for 1992–1995 and even slightly decrease for 1996–2000. To improve air quality, the Chinese government has implemented a large number of emission reduction measures to change the technology distribution and the emission factors after 1996 [*Lu et al.*, 2011]. The decline for 1996–2000 is also attributed to the slowdown in economic growth caused by the Asian economic crisis [*Ohara et al.*, 2007]. The post-2000 increase in BC emissions is driven by rapidly increasing energy consumption, industrial production, and vehicle population, which counteract the effect of technology improvements after 2000 [*Lu et al.*, 2011]. The complicated variations of anthropogenic BC emissions have been reported by many studies [e.g., *Streets et al.*, 2006, 2008; *Lu et al.*, 2011]. In China, the trend in anthropogenic BC emissions is controlled by the balance between a decreasing rate of emissions from the residential sector and an increasing rate of emissions from the industrial sector and diesel vehicles [*Ohara et al.*, 2007]. The residential and industrial emission sectors are the two major sources of BC in China, which account for 41–55% and 27–39% of the total BC emissions, respectively (summarized in *Li et al.*, [2016]).

Granier et al. [2011] summarized a number of anthropogenic emission inventories of BC in China and reported a general increase in emissions after 1980 in most inventories. They found that magnitudes and temporal trends of the emission inventories are different from 1980 to 2010, and the quantitative comparisons among different emission inventories are difficult, because of the different activity data and emission

factors used in estimating the emissions. In general, the magnitude of REAS emissions is in the middle of different BC emission inventories though the uncertainties may reach up to a factor of 1.8 [*Kurokawa et al.*, 2013]. From 1980 to 2010, the anthropogenic emissions of BC in REAS increase by 27% averaged over China, by 23% over eastern China, and by 63% over western China, respectively. Compared with other emission inventories, the REAS emissions might be higher in the 1980s but lower in the 2000s, representing the lower bound of the emission growth for 1980–2010. In other inventories, anthropogenic emissions of BC increase by 27% for 1980–2010 in *Bond et al.* [2007], by 45% for 1980–2010 in *Wang et al.* [2012], by 43% for 1980–2003 in *Junker and Liousse* [2008], by 64% for 1980–2006 in Aerosol Comparisons between Observations and Models (AEROCOM, http://dataipsl.ipsl.jussieu.fr/AEROCOM), and by 103% for 1980–2009 in *Qin and Xie* [2012]. The largest difference in temporal variations between REAS and other inventories is during the period of 1995–2000. BC emissions for 1995–2000 show a decrease in REAS and other studies, e.g., AEROCOM, *Bond et al.* [2007], and *Junker and Liousse* [2008], but the reduction is not evident in most inventories, e.g., Greenhouse Gas and Air Pollution Interactions and Synergies (http://gains.iiasa.ac.at/gains) and *Novakov et al.* [2003]. Note that the reduction for 1995–2000 in REAS is also consistent with most recent Chinese inventories, e.g., *Lu et al.* [2011], *Qin and Xie* [2012], and *Wang et al.* [2012].

Global biomass burning emissions of BC with a monthly temporal resolution are from the vegetation fire emission inventory for the Reanalysis of the Tropospheric chemical composition over the past 40 years project (RETRO) [*Schultz et al.*, 2008] (available at http://retro-archive.iek.fz-juelich.de/data/) for 1980–1996 and from the Global Fire Emissions Database version 3 (GFEDv3) [*van der Werf et al.*, 2010] for 1997–2010 (Figure 1). *Schultz et al.* [2008] reported that the geographical distribution and seasonal patterns of fires from RETRO agree reasonably well with those from an earlier version of the GFED inventory (GFEDv2) [*van der Werf et al.*, 2006]. The relationship between burned area from RETRO and carbon emissions from GFEDv2 is generally better than 0.8 for the continental-scale regions [*Schultz et al.*, 2008]. Consistently, we find that biomass burning emissions of BC in RETRO and GFEDv3 are in good agreement in Asia for 1997–2000, when both emission inventories are available (Figure 1). Biomass burning emissions for 1980–2010 are 12% of anthropogenic emissions in Asia and only 2% in China but show larger interannual variations than anthropogenic emissions.

The major uncertainties of biomass burning emissions lie in the estimates of burned area, fuel load, and emission factor [*Schultz et al.*, 2008; *van der Werf et al.*, 2010; *Randerson et al.*, 2012]. The uncertainties of global direct carbon emissions from RETRO in the 1980s and 1990s are approximately within ±50%. BC emissions are even more uncertain, by a factor of as much as 5 in some regions [*Schultz et al.*, 2008]. The uncertainty of the GFEDv3 emissions is at least 20% globally and higher in boreal regions and equatorial Asia [*van der Werf et al.*, 2010]. *Kaiser et al.* [2012] argued that GFEDv3 underestimates carbon emissions by a factor of 2–4 globally because of undetected small fires.

Wang et al. [2011] reported that anthropogenic emissions in Russia and Asia from *Bond et al.* [2007] for 2000 (~10% lower than those in REAS) are needed to be doubled to match BC surface observations in the Arctic. Modeled BC concentrations using the Intercontinental Chemical Transport Experiment Phase B inventory [*Zhang et al.*, 2009] for 2006 (about the same magnitude as those in REAS) are lower than those observed in Korea by a factor of 2, partially due to extremely low domestic anthropogenic emissions [*Jeong et al.*, 2011]. Comparing to a recent top-down estimates of BC emissions in China [*Fu et al.*, 2012], emissions in China from REAS are biased low by a factor of 2. We thus conduct a sensitivity simulation with doubled anthropogenic emissions in Asia from REAS, as described below.

2.1.3. Simulations
For the present study, we conduct the GEOS-Chem BC simulations for 1980–2010 driven by the MERRA meteorological fields. We perform the following simulations to identify the relative roles of variations in meteorological parameters and emissions in the decadal and interannual variations of BC in China (Table 1). All simulations are preceded by 1 year spin-up.

1. VALL is the simulation of BC with variations in both meteorological parameters and anthropogenic and biomass burning emissions over 1980–2010. This is the standard simulation, and the corresponding results are used in model evaluations in the present study unless stated otherwise.
2. VMET is the simulation to quantify the impact of variations in meteorological parameters alone on the decadal trend and interannual variation of BC. Meteorological parameters are allowed to vary over 1980–2010. Anthropogenic and biomass burning emissions are fixed at year 2010 levels.

Table 1. GEOS-Chem Simulations of BC

Model Experiments	Meteorological Parameters	Emissions	
		Anthropogenic	Biomass Burning
VALL	1980–2010	1980–2010	1980–2010
VMET	1980–2010	2010	2010
VEMIS	2010	1980–2010	1980–2010
VEMISAN	2010	1980–2010	Not included
VEMISBB	2010	Not included	1980–2010
VNOC	1980–2010	1980–2010	1980–2010
		turn off emissions in China	
VAN2X	1980–2010	1980–2010	1980–2010
		doubled in Asia	

3. VEMIS is the simulation to quantify the impact of variations in anthropogenic and biomass burning emissions on the decadal trend and interannual variation of BC. Meteorological parameters are fixed at year 2010 values. Anthropogenic and biomass burning emissions are allowed to vary over 1980–2010.

4. VEMISAN is the simulation to quantify the impact of variations in anthropogenic emissions alone on the decadal trend and interannual variation of BC. The model configurations are the same as those in VEMIS except that biomass burning emissions are not included.

5. VEMISBB is the simulation to quantify the impact of variations in biomass burning emissions alone on the decadal trend and interannual variation of BC. The model configurations are the same as those in VEMIS except that anthropogenic emissions are not included.

6. VNOC is the simulation to quantify the contribution of non-China emissions to BC in China. The model configurations are the same as those in VALL except that anthropogenic and biomass burning emissions in China are set to zero.

7. VAN2X is the model configurations that are the same as those in VALL except anthropogenic emissions of BC in Asia (10°S–55°N, 60°E–150°E) doubled.

To compare with observations, model results are sampled at the corresponding time and locations of the observed sites.

2.2. Observations

2.2.1. BC Concentrations in Surface Air

Ground-based measurements of BC concentrations are taken from the literature, as listed in Table 2. There are 20 sites with annual measurements of surface BC concentrations in China, which are distinguished based upon annual mean surface BC concentrations as reported by *Zhang et al.* [2008]. Five sites are located in rural regions, eight sites in remote areas, and seven sites in urban regions. The locations of the sites are shown in Figure 2. Observations are annual or multiyear averages during the period of 2000–2010, averaged over the years with measurements available.

2.2.2. BC Absorption Aerosol Optical Depth

There are 12 sites with absorption aerosol optical depth (AAOD) in China retrieved from the Aerosol Robotic Network (AERONET) [*Holben et al.*, 2001] (Table 3 and Figure 2). We infer BC AAOD from monthly averaged aerosol optical depth (AOD) data from AERONET (Version 2.0 Level 2.0 products, available at http://aeronet.gsfc.nasa.gov/) for 2002–2010, following *Bond et al.* [2013]. The annual means are derived for years when four or more months of monthly AOD observations are available. The aerosol column absorption is inferred from AOD and single-scattering albedo (SSA) via AAOD = AOD × (1 − SSA). We use AAOD at 550 nm by averaging retrievals calculated from 440 to 675 nm based on Ångström exponent. Both BC aerosols and dust particles contribute to the absorption. The absorption by fine-mode aerosols is primarily from BC, while the absorption by larger particles (diameter > 1 μm) is principally from dust. Dust AAOD is calculated from the AERONET retrieved size distribution and by a given refractive index of $1.55 + 0.0015i$. BC AAOD is thus estimated by separating dust AAOD from AERONET total AAOD. Because aerosol SSA retrievals are not reliable and not performed at low AODs [*Dubovik et al.*, 2002], the exclusion of low-AOD conditions in the AAOD retrieval likely introduces a positive bias [*Reddy et al.*, 2005]. The derived BC AAOD is likely biased high, too, because of the contributions from organic carbon and fine dust to fine-mode AAOD [*Bond et al.*, 2013].

Table 2. Observed and Simulated Annual Mean Surface BC Concentrations ($\mu g\ m^{-3}$) at 20 Sites in China[a]

| Site | Latitude (°N) | Longitude (°E) | Altitude (m) | Observation Period | BC Concentrations | | | Reference[d] |
					Observation	Model	NMB[e] (%)	
				Remote				
Akdala	47.1	88.0	562	2004.8–2005.3	0.35	0.23[b] (0.43[c])	−34 (23)	[1]
Zhuzhang	28.0	99.7	3583	2004.8–2005.2	0.34	0.19 (0.38)	−44 (12)	
Muztagh Ata	38.3	75.0	4500	2005	0.055	0.078 (0.15)	42 (173)	[2]
Nam Co	30.8	91.0	4730	2006.7–2007.1	0.082	0.064 (0.12)	−22 (46)	[3]
Waliguan	36.3	100.9	3616	2000–2010	0.30	0.15 (0.29)	−50 (−3)	[4]
				Rural				
Wusumu	40.6	112.6	1221	2005.9; 2006.12006.7; 2007.5	3.10	1.22 (2.41)	−61 (−22)	[5]
Gaolanshan	36.0	105.9	2075	2006–2007	3.77	0.98 (1.95)	−74 (−48)	[6]
Jinsha	29.6	114.2	424	2006–2007	2.98	2.00 (3.97)	−33 (33)	
Linan	30.3	119.7	149	2006–2007	4.24	1.73 (3.44)	−59 (−19)	
Longfengshan	44.7	127.6	337	2006–2007	2.25	1.48 (2.92)	−34 (30)	
Taiyangshan	29.2	111.7	571	2006–2007	2.61	2.00 (3.99)	−23 (53)	
Lanzhou	35.6	104.1	1966	2007.1–2009.8	1.59	1.10 (2.19)	−31 (38)	[7]
Maofengshan	23.3	113.5	550	2009	2.43	1.12 (2.19)	−54 (−10)	[8]
				Urban				
Chengdu	30.7	104.0	496	2006–2007	10.8	2.12 (4.22)	−80 (−61)	[6]
Dalian	38.9	121.6	92	2006–2007	5.3	1.48 (2.93)	−72 (−45)	
Gucheng	39.1	115.8	15	2006–2007	10.6	2.04 (4.06)	−81 (−62)	
Panyu	22.9	113.3	5	2006–2007	7.5	0.98 (1.92)	−87 (−74)	
Zhengzhou	34.8	113.7	99	2006–2007	9.4	2.70 (6.93)	−71 (−26)	
Xian	34.4	109.0	363	2006–2007	12.1	2.04 (4.07)	−83 (−66)	
Dongguan	23.0	113.5	30	2009	5.3	1.42 (2.79)	−73 (−47)	[7]

[a]Model results are from simulations VALL and VAN2X. See text and Table 1 for the definitions of model simulations.
[b]Results are from model simulation VALL.
[c]Results are from model simulation VAN2X.
[d]Sources are the following: [1] *Qu et al.* [2008]; [2] *Cao et al.* [2009]; [3] *Ming et al.* [2010]; [4] *Zhao et al.* [2014]; [5] *Han et al.* [2008]; [6] *Zhang et al.* [2012]; [7] *Zhang et al.* [2011]; and [8] *Chen et al.* [2013].
[e]Normalized mean biases (NMB) = 100% × (Model − Observation)/Observation, where Model and Observation are the simulated and observed BC concentrations, respectively.

2.2.3. BC Concentrations in Ice Cores and Lake Sediments
There are seven sites with annual measurements of historical BC in ice cores [*Xu et al.*, 2009] or in lake sediments [*Han et al.*, 2011] for 1980–2006 (Figure 2). BC concentrations in ice cores were measured at five
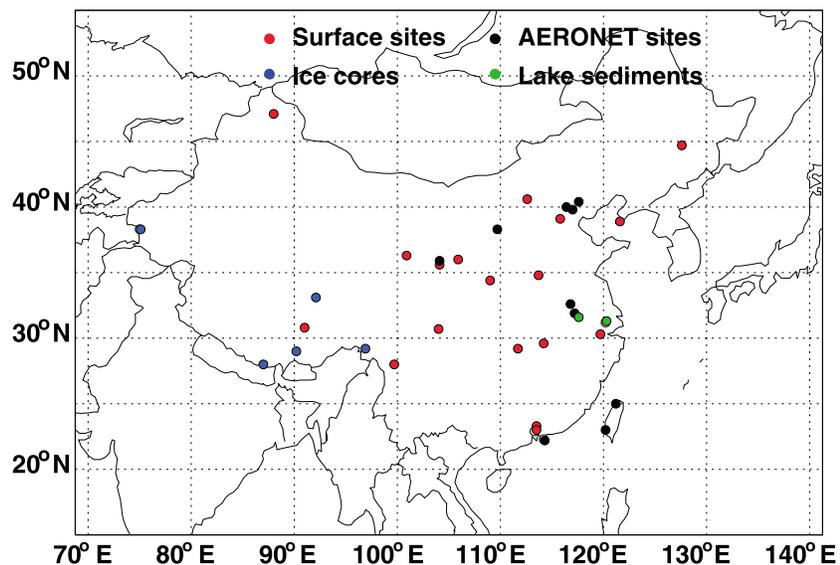
Figure 2. Locations of BC measurements in China used in the present study.

Table 3. AERONET-Derived and GEOS-Chem-Simulated Annual Mean BC Absorption Aerosol Optical Depth (AAOD) at 12 AERONET Sites in China[a]

					BC AAOD		
Site	Latitude(°N)	Longitude(°E)	Altitude(m)	Time	Observation	Model	NMB[d] (%)
Rural							
Taihu	31.2	120.2	20	2006–2010	0.054	0.021[b] (0.041[c])	−61 (−24)
SACOL	35.9	104.1	1965	2006–2010	0.031	0.010 (0.019)	−68 (−39)
Xinglong	40.4	117.6	970	2006–2010	0.037	0.027 (0.053)	−27 (43)
Shouxian	32.6	116.8	22	2008	0.038	0.021 (0.040)	−45 (5)
Hefei	31.9	117.2	36	2008	0.047	0.026 (0.050)	−45 (6)
Xianghe	39.8	117.0	36	2005–2010	0.058	0.027 (0.052)	−53 (−10)
Urban							
Beijing	40.0	116.4	92	2002–2010	0.065	0.026 (0.050)	−60 (−23)
Yulin	38.3	109.7	1080	2002	0.061	0.010 (0.019)	−84 (−69)
HK_PolyU	22.3	114.2	30	2006–2010	0.062	0.008 (0.017)	−87 (−73)
HK_Hok_Tsui	22.2	114.3	80	2008–2010	0.045	0.010 (0.018)	−78 (−60)
Chen-kung	23.0	120.2	50	2004–2010	0.025	0.006 (0.010)	−76 (–60)
NCU	25.0	121.2	171	2002–2010	0.030	0.005 (0.009)	−83 (−70)

[a]Model results are from simulations VALL and VAN2X. See text and Table 1 for the definitions of model simulations.
[b]Results are from model simulation VALL.
[c]Results are from model simulation VAN2X.
[d]Normalized mean biases (NMB) = 100% × (Model − Observation)/Observation, where Model and Observation are the simulated and derived BC AAOD, respectively.

elevated (>5600 m above sea level) and remote sites in the Tibetan Plateau [cf. *Xu et al.*, 2009, Figure 1]. The ice samples taken from these sites were melted and immediately filtered through prefired quartz fiber filters. BC on the filters was measured by using the IMPROVE thermal/optical reflectance (TOR) protocol [*Chow et al.*, 2004]. The uncertainty of BC measurements is about 15% considering all the possible effects, e.g., the separation of BC fractions and influence of dust particles on laser reflection. BC mass accumulation rates in lake sediments were measured in Lakes Chaohu (31.4–31.7°N, 117.3–117.9°E) and Taihu (30.9–31.6°N, 119.9–120.6°E), located in the delta of the Yangtze River in eastern China [cf. *Han et al.*, 2011, Figure S1]. Sediment samples were oven dried at 40°C for approximately 144 h and measured for BC by using the TOR method. The uncertainty of the TOR method is < 10% for BC measurements in the two lakes.

3. Simulated BC and Model Evaluation

3.1. Simulated Spatiotemporal Distributions of BC

Figure 3a shows the spatial distributions of simulated seasonal mean surface BC concentrations in China from simulation VALL for 2010. High BC concentrations are simulated in eastern China, with the highest values (>4 μg m^{-3}) in the densely populated and heavily industrialized areas, such as the Northeastern China Plain, the Sichuan Basin, and the Yangtze River Delta and Pearl River Delta megacity clusters. Model-simulated surface BC concentrations show strong seasonal variations. Mean surface BC concentrations averaged over China range from 0.67 μg m^{-3} in summer (June-July-August) to 1.77 μg m^{-3} in winter (December-January-February, DJF) in the VALL simulation. Similar seasonal variations of surface BC concentrations were reported by many previous studies [e.g., *Fu et al.*, 2012; *Zhang et al.*, 2012]. Model simulation results with/without seasonal variations in emissions indicate that both the strong anthropogenic emissions from heating [*Fu et al.*, 2012; *Lu et al.*, 2011] and the changes in meteorological parameters (e.g., boundary layer compression in winter or enhanced wet deposition in summer) [*Fu et al.*, 2012] are important factors contributing to the high concentrations during the cold months.

Also shown in Figure 3b are the differences in simulated seasonal mean surface BC concentrations between 2010 and 1980. We find that the large differences are located in the densely populated areas in eastern China, with large increases > 2.5 μg m^{-3} in winter. The differences are largely because of the rapid increase of emissions in the region. Relative to 1980, surface BC concentrations in 2010 increase by 0.29 μg m^{-3} (24%) averaged over eastern China and by 0.12 μg m^{-3} (66%) over western China, consistent with the enhancements of anthropogenic emissions (section 2.1.2).

3.2. Evaluation of Simulated Surface Layer BC Concentrations

We evaluate simulated annual mean surface BC concentrations by using the observations from the 20 ground sites in Table 2. For comparisons, both simulated and observed concentrations are averaged over the years
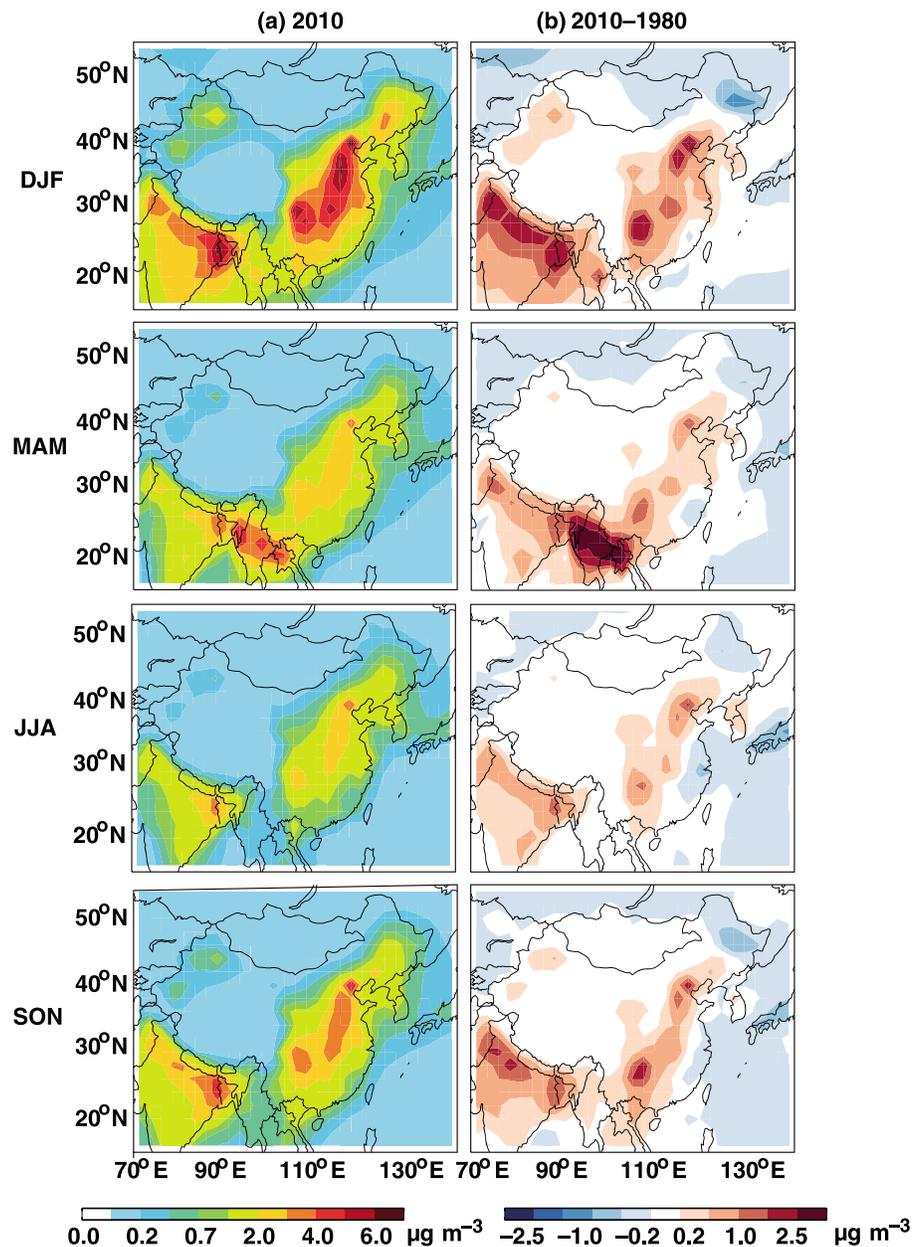
Figure 3. (a) Simulated seasonal mean surface BC concentrations ($\mu g\,m^{-3}$) in China for 2010. (b) Differences in simulated seasonal mean surface BC concentrations ($\mu g\,m^{-3}$) in China between 2010 and 1980. Results are from model simulation VALL.

with measurements available. Model results from the standard simulation VALL generally underestimate observed BC concentrations at most of the sites, except at Muztagh Ata. Model-simulated BC concentrations show normalized mean biases (NMB) of −37% at remote sites, −49% at rural sites, and −79% at urban sites,. The comparisons between simulated and observed BC concentrations are in better agreement at remote sites than at rural sites, as rural sites are closer to the urban regions and more influenced by strong emission sources. Our results are consistent with those from *Fu et al.* [2012] and *Jeong et al.* [2011], which attributed the low biases to the underestimated BC emissions in Asia. We find that model simulation with doubled BC emissions in Asia significantly improves the model versus observation comparisons. The resulting BC concentrations are in better agreement with observations at most of the sites and have a NMB of 1% at remote and rural sites. The simulated surface BC concentrations in VAN2X increase approximately twice as high at most of the sites, compared with those in VALL. This linear enhancement is because anthropogenic emissions are the major source of surface BC concentrations in China (Figures 1 and 7).
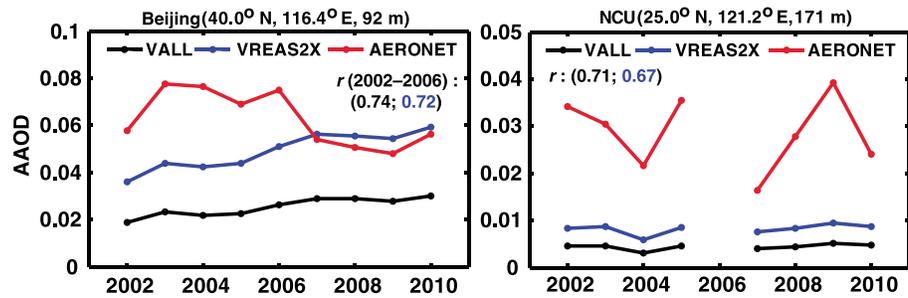
Figure 4. AERONET-derived and GEOS-Chem-simulated annual mean BC absorption aerosol optical depth (AAOD) at Beijing and NCU for 2002–2010. Model results are from simulations VALL and VAN2X. Also shown are the correlation coefficients (*r*) between AERONET-derived and simulated BC AAOD.

3.3. Evaluation of Simulated BC AAOD

Table 3 compares AERONET-derived and GEOS-Chem-simulated annual mean BC AAOD at 12 AERONET sites in China. We sample model results from simulations VALL and VAN2X at the time and location of
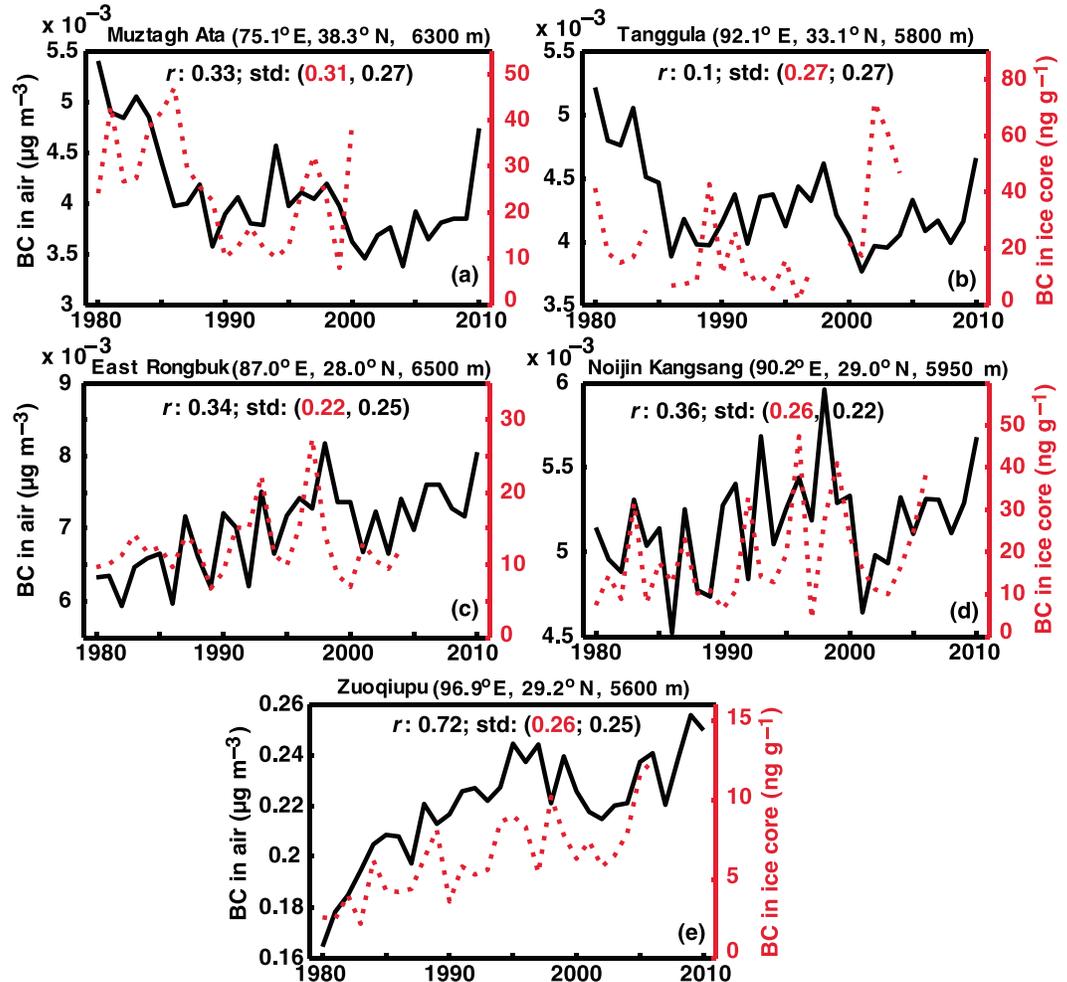
Figure 5. Observed annual BC concentrations (red, right *y* axis, ng g^{-1}) in ice cores in the Tibetan Plateau [*Xu et al.*, 2009] and simulated annual mean BC concentrations (black, left *y* axis, μg m^{-3}) in the (a–d) atmosphere at 300 hPa and in (e) surface air for 1980–2010. Also shown are the correlation coefficients (*r*) between observed and simulated BC concentrations and standard deviations of min-max normalization of observed and simulated BC concentrations. Model results are from simulation VALL.
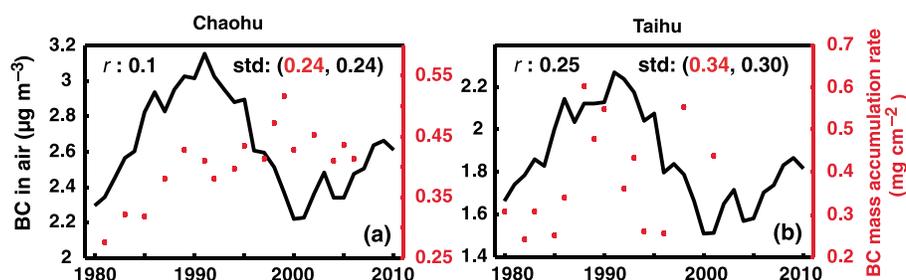
Figure 6. Observed annual BC mass accumulation rate (red, right *y* axis, mg cm^{-2}) in lake sediments of Lakes (a) Chaohu and (b) Taihu in eastern China [*Han et al.*, 2011] and simulated annual mean BC concentrations (black, left *y* axis, μg m^{-3}) in surface air for 1980–2010. Also shown are the correlation coefficients (*r*) between observed and simulated BC and standard deviations of min-max normalization of observed and simulated BC. Model results are from simulation VALL.

observations. Compared to the derived AAOD, model-simulated annual mean BC AAOD in simulation VALL (VAN2X) show NMB values of −77% (−57%) at urban sites and −50% (−4%) at remote sites. The simulated BC AAOD values in VAN2X are roughly 2 times of those in VALL, similar to the simulated surface BC concentrations in the two simulations (section 3.2). The large discrepancies between derived and simulated BC AAOD are also found in many studies [e.g., *Q. Wang et al.*, 2014], which can be largely attributed to the uncertainties in the AERONET retrievals [*Dubovik et al.*, 2002; *Reddy et al.*, 2005; *Bond et al.*, 2013]. The total AAOD retrievals are likely biased high by a factor of 2 because of the exclusion of low-AOD conditions [*Reddy et al.*, 2005]. *Bond et al.* [2013] have shown that derived BC AAOD can be biased high by 40–50% due to the contributions from organic carbon and fine dust. In addition, the MAC used in the calculation of BC AAOD in GEOS-Chem is 7.5 m^2 g^{-1} at 550 nm, which is much lower than 11.3 m^2 g^{-1} recommended by *Bond et al.* [2013]. An increase of MAC from 7.5 to 11 m^2 g^{-1} in BC AAOD calculation using the GEOS-Chem model would reduce the NMBs by 11% at urban sites and by 23% at remote sites. Moreover, since many of the AERONET sites are located in or near large cities and therefore severely influenced by strong local emissions, the coarse resolution of the GEOS-Chem model is thus another important factor that accounts for the above-mentioned discrepancies between derived and simulated BC AAOD.

We also compare in Figure 4 AERONET-derived and GEOS-Chem-simulated annual mean BC AAOD at Beijing and NCU for 2002–2010. The correlation coefficients between AERONET-derived and simulated BC AAOD are ~0.7 at Beijing for 2002–2006 and at NCU for 2002–2010. Model fails to capture the decreased AERONET AAOD at Beijing in the late 2000s. Note that large uncertainties exist in the retrieved AAOD as discussed above. In addition, the projected emissions used in the coarse-resolution model are likely not accurate enough in the Beijing urban area.

3.4. Comparisons With Measured BC in Ice Cores and Lake Sediments

We also evaluate the ability of the GEOS-Chem model to capture the decadal and interannual variations of BC in China using historical BC in ice cores in the Tibetan Plateau (Figure 5) and in lake sediments in eastern China (Figure 6) for 1980–2006. Because GEOS-Chem model is lack of a land surface model, we thus do not attempt to reproduce the observed BC concentration in ice cores or lake sediments, focusing instead on the ability of GEOS-Chem to accurately represent long-range transport of pollution and decadal and interannual variations of BC in China. *Ming et al.* [2008] have shown that atmospheric BC concentrations are strongly correlated with wet-deposited BC concentrations in ice via wet scavenging ratio method following *Davidson et al.* [1993]. As studies estimated between 80% and 98% of BC is removed through wet deposition [*Jacobson*, 2004; *Textor et al.*, 2006; *He et al.*, 2014], we assume that wet deposition dominates BC aerosol removal from the atmosphere in this study. Therefore, here we compare simulated annual mean BC concentrations in the atmosphere with observed annual BC in ice cores and lake sediments. *Han et al.* [2011] also suggested that the temporal trends of BC in lake sediments reasonably reflect the variations of regional BC pollution.

Figure 5 shows observed annual BC concentrations in five ice cores. We distinguish the five sites based on the studies about the pathways of BC in the Tibetan Plateau [*Xu et al.*, 2009; *Kopacz et al.*, 2011]. The southern plateau includes East Rongbuk glacier (Mount Everest, 28.0°N, 87.0°E, 6500 m), Noijin Kangsang glacier

(29.0°N, 90.2°E, 5950 m), and Zuoqiupu glacier (29.2°N, 96.9°E, 5600 m) and receives BC depositions mainly from India and China. Mount Muztagh Ata (38.3°N, 75.1°E, 6300 m) locates in the northern plateau and is under control of the westerlies throughout the year, and its upwind sources are principally from western China, the Middle East, and Europe. Tanggula glacier (33.1°N, 92.1°E, 5800 m) locates in the central plateau and is in the interactional area of the westerly winds and the South Asian monsoon.

The variations of BC deposited in the Tibetan Plateau depend on meteorology and major BC sources. In Figure 5, observed annual BC concentrations in ice cores are increasing from 1980 at the three southern glaciers, which are consistent with the increasing anthropogenic emissions in Asia. There is a sharp decrease in observed BC concentrations at Mount Muztagh Ata and Tanggula glacier in the late 1980s. The decline is likely because of the significantly decreased anthropogenic emissions in Europe [*Bond et al.*, 2007; *Granier et al.*, 2011]. We find that observed BC concentrations are increasing again after 2000, due to the rapid increase of anthropogenic BC emissions in Asia. The differences in observed BC concentrations between the southern and northern glaciers reflect the above-mentioned differences in source regions and transport pathways.

Also shown in Figure 5 are simulated BC concentrations at the corresponding sites. Hereinafter, we use model simulation VALL instead of VAN2X to quantify the variations of BC in the present study, as model-simulated surface concentrations and column burdens of BC in VAN2X are roughly 2 times of those in VALL (sections 3.2 and 3.3) and simulated BC in VAN2X and VALL shows similar decadal and interannual variations. We find that simulated surface concentrations at Zuoqiupu and model results at 300 hPa at other four sites show best comparisons with observations. At Zuoqiupu, we compare the simulated BC concentrations in surface air with the observations, as the site is the most representative of Chinese sources among the five sites [*Kopacz et al.*, 2011; *M. Wang et al.*, 2014]. Model results at 300 hPa are most representative of the variations of observed BC concentrations at the four sites, as the sites are located in the Tibetan Plateau with high elevations, where the coarse-resolution model is difficult to represent due to complex topography and meteorology [e.g., *Mao et al.*, 2011; *He et al.*, 2014].

Our simulated BC concentrations in the atmosphere reasonably capture the interannual variations of observed BC concentrations in ice cores. Model-simulated BC concentrations at the three southern sites increase from 1980 in VALL, consistent with the corresponding observations. Simulated BC concentrations capture the observed declines at the three southern sites in the late 1990s and at Mount Muztagh Ata and Tanggula glacier in the late 1980s. The standard deviations of min-max normalization of simulated annual mean values of BC are close to those of observed values at individual sites, and the differences are within 14%. The correlation coefficients between simulated and observed BC are consistently larger than 0.3, except at Tanggula. Among the five sites, the best agreement between observed and simulated BC is located at Zuoqiupu ($r = 0.72$), which is severely influenced by Asian sources [*Xu et al.*, 2009]. The worse comparisons between observed and simulated BC at other four sites are likely because of the factors, e.g., inaccurate representation of long-range transport in the model or absence of detailed annual emissions in the Middle East and Europe in the present study. At Tanggula, model fails to capture the observed BC peaks around 1990 and 2005, indicating that model likely lacks the ability to accurately represent the transport of Asian pollutant via South Asian monsoon at the site.

Figure 6 compares simulated annual mean BC concentrations in surface air versus observed annual BC mass accumulation rate in the lake sediments of Lakes Chaohu and Taihu [*Han et al.*, 2011] for 1980–2010. The standard deviations of min-max normalization of simulated (observed) annual mean values of BC are 0.24 (0.24) at Lake Chaohu and 0.30 (0.34) at Lake Taihu, respectively. The correlation coefficients between simulated and observed BC are 0.25 at Lake Taihu and 0.1 at Lake Chaohu, respectively, showing that simulated BC concentrations are in poor agreement with observations. Better comparisons between observed and simulated BC in Lake Taihu than in Lake Chaohu might because Lake Taihu is in the more industrialized region in the past 30 years [*Han et al.*, 2011]. Model-simulated surface BC concentrations capture the observed BC peaks in 1990 at Lake Taihu, but model results miss the observed peak around 2000 at Lake Chaohu. The discrepancies between observed and modeled surface BC are likely due to the uncertainties of the BC measurement in the lake sediments and those within the model. For example, the uncertainties in the estimated ages of samples are about 1–3 years [*Han et al.*, 2011]. In addition, atmospheric deposition is not the only pathway of BC in lake sediments. BC enters waters also through riverine inputs and surface runoff [*Han et al.*, 2011]. The inaccurate emissions used in the model are another important factor that accounts for the above-mentioned discrepancies.
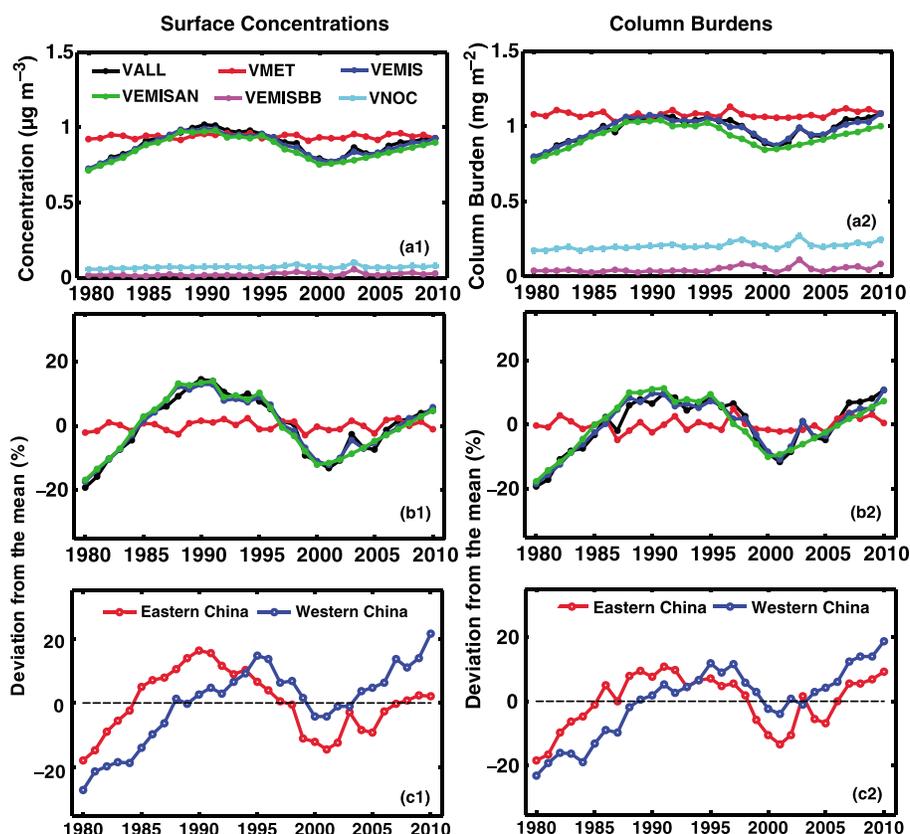
Figure 7. (a1) Annual mean surface concentrations ($\mu g\,m^{-3}$) and (a2) tropospheric column burdens ($mg\,m^{-2}$, below 10 km) of BC averaged over China from model simulations VALL (black), VMET (red), VEMIS (blue), VEMISAN (green), VEMISBB (pink), and VNOC (light blue) for 1980–2010. Deviation from the mean (DM, %) of (b1) annual mean surface concentrations and (b2) tropospheric column burdens of BC averaged over China from model simulations VALL (black), VMET (red), VEMIS (blue), and VEMISAN (green). DM (%) of (c1) annual mean surface concentrations and (c2) tropospheric column burdens of BC averaged over eastern China (red, east of 105°E) and western China (blue, west of 105°E) from simulation VALL. See text for the definition of DM.

4. Simulated Decadal Trends of BC

The above-mentioned evaluations of model results prove the ability of the GEOS-Chem model to reasonably capture the decadal and interannual variations of BC in China. Figure 7a shows simulated annual mean surface concentrations and tropospheric column burdens (below 10 km) of BC for 1980–2010 averaged over China. In the VALL simulation, model-simulated annual mean surface concentrations (column burdens) of BC are in the range of ~0.7–1.0 $\mu g\,m^{-3}$ (~0.8–1.1 $mg\,m^{-2}$) averaged over China. Relative to year 1980, the annual mean surface BC concentrations in year 2010 increase by 0.21 $\mu g\,m^{-3}$ (29%) averaged over China. The corresponding difference between 2010 and 1980 in column burdens of BC is 0.29 $mg\,m^{-2}$ (37%). We find that the variations of surface BC concentrations for 1980–2010 are similar to the changes of column burdens of BC, which are generally consistent with the changes of anthropogenic emissions used in the model. Simulated BC increase in the 1980s and 2000s and decrease in the late 1990s. Note that our simulations are significantly dependent on the variations of the REAS inventory; large biases thus exist in the variations of simulated BC because of the uncertainties in the REAS inventory as discussed in section 2.1.2.

We calculate in the present study the decadal trends in simulated BC using the least squares fit for 1980–1989, 1990–1999, and 2000–2010. All the calculated decadal trends pass the two-tailed t test with 99% confidence. The resulting decadal trends in annual mean surface BC concentrations are 0.31 $\mu g\,m^{-3}\,decade^{-1}$ in the 1980s, −0.20 in the 1990s, and 0.16 in the 2000s. The corresponding decadal trends in column burdens of BC are 0.29, −0.10, and 0.21 $mg\,m^{-2}\,decade^{-1}$. The variations of BC in simulation VEMIS are similar to those in simulation VALL, indicated that changes in emissions are the major factor that contributes to the decadal
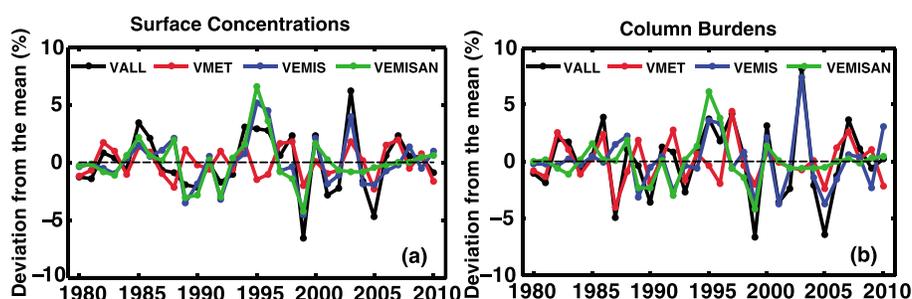
Figure 8. Deviation from the mean (DM, %) of the (a) detrended annual mean surface concentrations and (b) tropospheric column burdens of BC averaged over China for 1980–2010. Results are from model simulations VALL (black), VMET (red), VEMIS (blue), and VEMISAN (green). The decadal trends in BC are calculated using the least squares fit approach for every 10 years and removed from each decade. See text for the definition of DM.

trends of both surface concentrations and column burdens of BC in China. We find that the simulated BC in VEMIS and VEMISAN show similar variations because anthropogenic emissions are the major source of BC in China (Figure 1), accounting for approximately 98% (95%) of the simulated surface concentrations (column burdens) of BC. For simulation VMET, we find no obvious decadal trends in the simulated BC. In each simulation, the decadal trends of simulated BC are similar among the four seasons (not shown).

Also shown in Figure 7a are simulated surface concentrations and tropospheric column burdens of BC from model simulation VNOC. The percentage contributions of non-China emissions are 8% to surface concentrations of BC and 21% to column burden of BC. The contributions of non-China emissions to column burdens of BC increase by 0.016 mg m^{-2} decade^{-1} (9% decade^{-1}) in the past 30 years, largely because of the increasing emissions from India.

We calculate in Figure 7b the deviation from the mean (DM) of simulated annual mean surface concentrations and column burdens of BC averaged over China for 1980–2010. Following the studies, e.g., *Mu and Liao* [2014] and *Yang et al.* [2015], DM is defined as

$$DM_i = \left(M_i - \frac{1}{n}\sum_{i=1}^{n} M_i \right) / \frac{1}{n}\sum_{i=1}^{n} M_i, \qquad (1)$$

where M_i is the simulated annual mean BC in China for year i, and n is the number of years examined ($n = 31$ for years 1980–2010). The variations of DM values for simulated BC show similar patterns to the variations of the corresponding simulated BC in each simulation. The values of DM for annual mean surface concentrations (column burdens) of BC in simulation VALL are in the range of −20% to 15% (−20% to 11%) averaged over China, which peak at ~15% (~10%) around 1990 and decrease to −13% (−12%) at 2000. The variations in DM values in simulation VALL are in good agreement with those in VEMIS. The deviations in surface concentrations (column burdens) of BC in simulation VMET are within −3% to 3% (−5% to 5%), which are much smaller than those in VALL and VEMIS. The DM values in VALL, VEMIS, and VMET again suggest that the decadal trends of both surface concentrations and column burdens of BC are largely dependent on variations in emissions.

Figure 7c compares the DM values of simulated annual mean surface concentrations and column burdens of BC averaged over eastern and western China in simulation VALL for 1980–2010. The variations in DM values for annual mean surface BC concentrations are larger averaged over western China (−27% to 21%) than over eastern China (−18% to 16%). The DM values of column burdens of BC are −23% to 19% averaged over western China and −18% to 11% in eastern China. Simulated surface concentrations and column burdens of BC show similar temporal variations. Simulated BC averaged over eastern China shows increases in the 1980s and 2000s and a decline in the 1990s, while simulated BC in western China shows increases before 1995 and after 2000. The decadal trends in annual mean surface BC concentrations averaged over eastern China are 0.52, −0.38, and 0.25 μg m^{-3} decade^{-1}, respectively, in the 1980s, 1990s, and 2000s. The corresponding values averaged over western China are much smaller and are 0.07, −0.09, and 0.06 μg m^{-3} decade^{-1}. Compared to the year 1980, model-simulated surface BC concentrations in 1990 increase by 39% in eastern China and by 37% in western China. The increasing rate of surface BC concentrations between 2010 and 2000 is higher in western China than in eastern China (27% versus 16%). The variations of simulated BC in eastern and western China are similar to the changes in the anthropogenic emissions in the corresponding regions

(Figure 1). The differences in the simulated BC between eastern and western China are thus mainly caused by the regional differences in economic development, industry structure, and population [*Zhang et al.*, 2009].

5. Simulated Interannual Variations of BC

To analyze the interannual variations of BC, the decadal trends in the simulated BC are firstly identified by linear square fit for every 10 years (as shown in section 4) and removed from each decade, based on the approach used in previous studies [e.g., *Yang et al.*, 2015]. We quantify the impact of changes in emissions and meteorological parameters on the interannual variations of surface concentrations and column burdens of BC by using DM, mean absolute deviation (MAD), and absolute percent departure from the mean (APDM) [e.g., *Mu and Liao*, 2014; *Yang et al.*, 2015]. The latter two indexes are defined as

$$MAD = \frac{1}{n} \sum_{i=1}^{n} \left| M_i - \frac{1}{n} \sum_{i=1}^{n} M_i \right|, \tag{2}$$

$$APDM = 100\% \times MAD / \left(\frac{1}{n} \sum_{i=1}^{n} M_i \right), \tag{3}$$

where M_i is the detrended simulated annual mean BC in China for year i, and n is the number of years examined. Therefore, MAD and APDM (or DM) represent the interannual variations of BC in terms of absolute value and percentage, respectively, averaged over the 31 years for 1980–2010 in the present study.

Figure 8 shows the DM values of detrended simulated annual mean surface concentrations and column burdens of BC for 1980–2010. The DM values in surface BC concentrations are −7% to 6% in VALL, −2% to 2% in VMET, −4% to 5% in VEMIS, and −4% to 7% in VEMISAN. The DM values in VMET are larger in column burdens of BC (−4% to 4%) than in surface concentrations. In other simulations VALL, VEMIS, and VEMISAN, the variations in column burdens of BC are similar to the corresponding changes in surface concentrations. The deviations of both surface concentrations and column burdens of BC in simulations VALL are comparable to those in VMET, VEMIS, and VEMISAN. We find that the peaks and troughs in deviations in VALL simulation are consistent with those in either VMET or VEMIS, suggesting that the interannual variations of surface concentrations and column burdens of BC are dependent on changes in both meteorological parameters and emissions. Meteorological parameters are a more important impact factor to column burdens of BC than to surface concentrations. The interannual variations of BC due to changes of anthropogenic emissions alone (VEMISAN) are similar to those due to changes of both anthropogenic and biomass burning emissions (VEMIS) (except in 2003), due to the significant large anthropogenic emissions.

Figure 9 compares the APDM values of detrended simulated annual mean surface BC concentrations in China for 1980–2010 from model simulations VALL, VMET, VEMIS, and VEMISAN. In each simulation, the spatial distributions of APDM values of surface BC concentrations are similar to those of column burdens of BC (not shown). In simulation VALL, the interannual variations of surface BC concentrations are 0.014 μg m^{-3} (2.0%) for MAD (APDM) averaged over China. Regionally, the APDM values of surface BC concentrations are 2–6% over eastern China and > 6% in western China. We find that the APDM values in VMET and VEMIS are comparable in southeastern China (~2%) and in northwestern China (~4%), indicating that both meteorological parameters and emissions are important in driving the variations of surface BC concentrations in the two regions. In northeastern China, the interannual variations are more dependent on the changes of meteorological parameters (~4% versus < 2% in VEMIS). The large interannual variations in VALL are found in the Tibetan Plateau, with a maximum APDM value exceeding 8%, which are largely driven by the changes in meteorological parameters (>4% in VMET versus < 2% in VEMIS). The interannual variations of surface BC concentrations in simulations VEMIS and VEMISAN show similar spatial distribution and magnitude in most of China, except at regions close to the biomass burning sources, e.g., southern Yunnan province and northern Heilongjiang and Neimenggu provinces.

To compare with the interannual variations of surface BC estimated by *Mu and Liao* [2014], we calculate the APDM values for 2004–2010 averaged over three regions in eastern China (cf. Figure 1) [*Mu and Liao*, 2014]. *Mu and Liao* [2014] reported that the interannual variations of BC in eastern China are about 6–14% for 2004–2012 and are largely dependent on variations in meteorological parameters. Our analyses for 2004–2010 show that the interannual variations of BC are about 2–8% in the eastern China, which are influenced by changes in meteorological
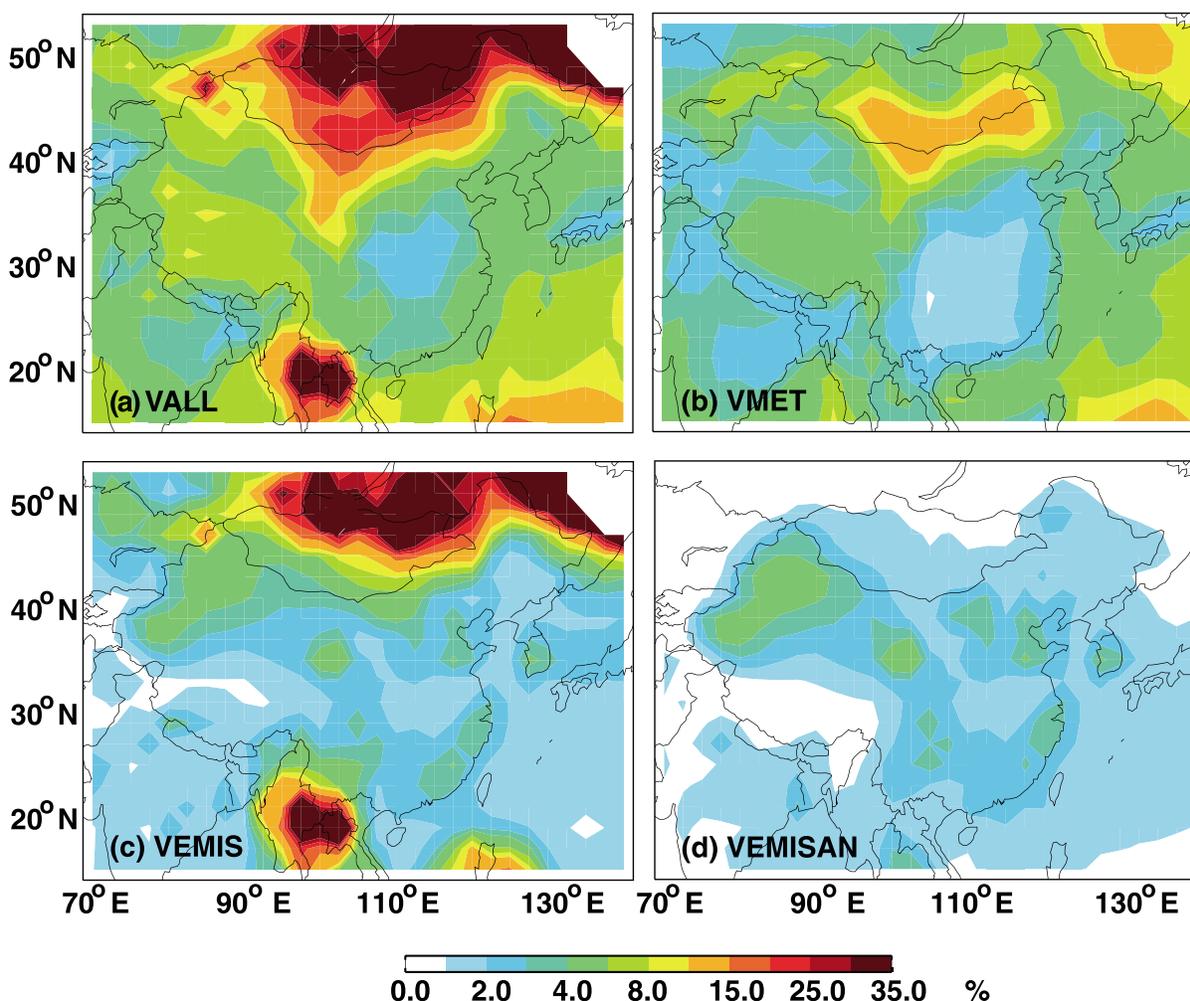
Figure 9. Simulated absolute percent departure from the mean (APDM, %) of the detrended annual mean surface BC concentrations in China for 1980–2010. Results are from model simulations (a) VALL, (b) VMET, (c) VEMIS, and (d) VEMISAN. See definitions of APDM in the text.

parameters and emissions. This discrepancy between the two studies is largely because of the different metrological fields and emission inventory used in estimating the interannual variations of BC.

In Figure 10, we summarize the MAD and APDM values of the detrended seasonal and annual mean surface concentrations and column burdens of BC averaged over China for 1980–2010. The variations of simulated annual mean surface concentrations (column burdens) of BC averaged over China are $0.068\,\mu g\,m^{-3}$ $(0.069\,mg\,m^{-2})$ for MAD and 7.7% (7.1%) for APDM, without removing the linear trend. The detrended APDM and MAD values of surface concentrations (column burdens) of BC are 2.5–4.2% (3.4–4.9%) and 0.013–0.034 $\mu g\,m^{-3}$ (0.024–0.038 $mg\,m^{-2}$) in simulation VALL, with the maximum values in DJF and March-April-May (MAM). We find that the MAD and APDM values in VMET and VEMIS are generally comparable, indicating again that the interannual variations in surface concentrations and column burdens of BC are driven by variations in both meteorological parameters and emissions. In DJF, meteorological parameters are more important in driving the interannual variations of BC, as both MAD and APDM values in VMET are 2 times of those in VEMIS. Annually, the MAD and APDM values of surface concentrations (column burdens) of BC due to changes in anthropogenic alone (VEMISAN) are ~ 90% (70%) of those due to variations in both anthropogenic and biomass burning emissions (VEMIS). The interannual variations of surface concentrations (column burdens) of BC due to biomass burning emissions are largest in MAM, as anthropogenic emissions only account for ~42% (28%) of the interannual variations of BC in VEMIS. The influences of non-China emissions on BC are also largest in MAM.
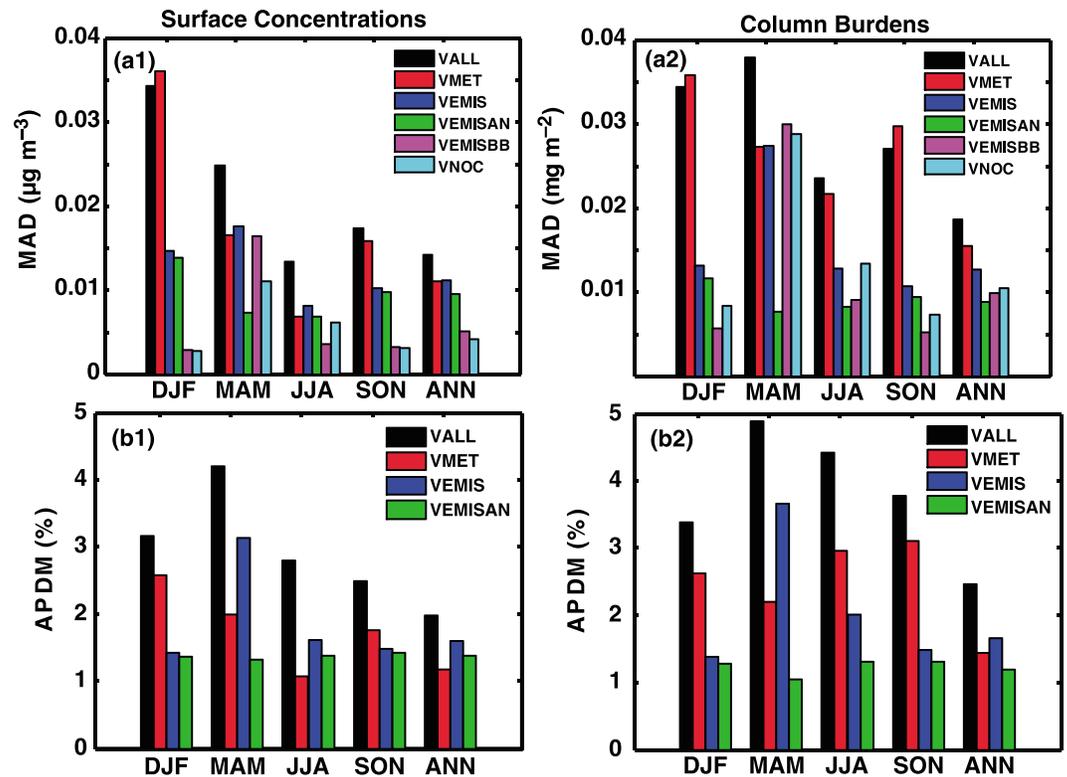
Figure 10. Mean absolute deviation (MAD, $\mu g\,m^{-3}$) of the (a1) detrended seasonal and annual mean surface concentrations and (a2) tropospheric column burdens of BC in China for 1980–2010. Results are from model simulations VALL (black), VMET (red), VEMIS (blue), VEMISAN (green), VEMISBB (pink), and VNOC (light blue). Absolute percent departure from the mean (APDM, %) of the (b1) detrended seasonal and annual mean surface concentrations and (b2) tropospheric column burdens of BC in China for 1980–2010. Results are from model simulations VALL (black), VMET (red), VEMIS (blue), and VEMISAN (green). See definitions of MAD and APDM in the text.

Variations in meteorological parameters influence interannual variations of surface BC concentrations mainly by the changes in deposition and transport [*Mu and Liao*, 2014], as well as by the variability of biomass burning emissions [*Schultz et al.*, 2008]. Local meteorological conditions (e.g., wind speed and mixing depth) also influence surface BC [*Zhu et al.*, 2012; *Mu and Liao*, 2014]. Following the process analyses used in *Mu and Liao* [2014], we calculate the MAD values of horizontal and vertical transport and wet and dry deposition of BC in China (85–120°E, 20–45°N, from the surface to 1 km) in VMET. The relative contributions of the MAD values of the horizontal transport, vertical transport, wet deposition, and dry deposition of BC to the sum of the MADs from the four processes are 44%, 20%, 29%, and 7%, respectively. Wind is thus the major meteorological factor to influence the interannual variations of surface BC. For column burdens of BC, the relative contributions of the MAD values of the four processes are 31%, 35%, 31%, and 3%. Horizontal and vertical transport and wet deposition are thus important meteorological factors that drive the interannual variations of column burdens of BC.

6. Direct Radiative Forcing of BC

Figure 11 shows simulated annual mean all-sky TOA DRF of BC averaged over China in 1980, 1985, 1990, 1995, 2000, 2005, and 2010. The variations of BC DRF are similar to the changes in tropospheric column burden of BC (Figure 7a), with the maximal value in 2010 ($1.03\,W\,m^{-2}$) and minimal value in 1980 ($0.68\,W\,m^{-2}$). Annual mean BC DRF averaged over China increases by $0.35\,W\,m^{-2}$ (51%) from 1980 to 2010. The increases are significant comparing to the global annual mean DRF values of BC ($0.4\,W\,m^{-2}$), tropospheric ozone ($0.4\,W\,m^{-2}$), and carbon dioxide ($1.82\,W\,m^{-2}$) reported by *IPCC* [2013]. Our simulated TOA DRF of BC in China is in the middle range of previous estimates ($0.58–1.46\,W\,m^{-2}$, summarized in *Li et al.* [2016]). We note that simulated DRF is associated with large uncertainties resulting from factors including BC mixing state, emissions, vertical distribution, wet scavenge scheme (lifetime), and MAC used in the model. For example, the differences in DRF
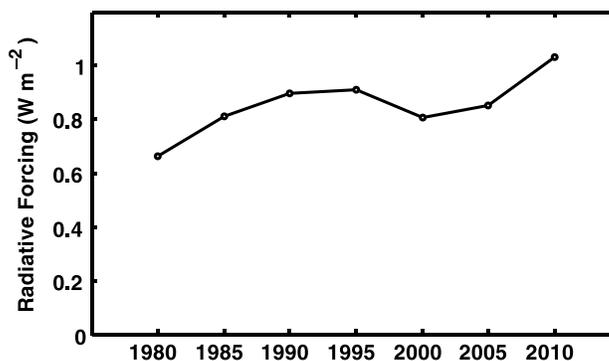
Figure 11. Simulated annual mean all-sky direct radiative forcing (DRF) of BC (W m^{-2}) at the top of the atmosphere (TOA) averaged over China in 1980, 1985, 1990, 1995, 2000, 2005, and 2010.

between 2010 and 1980 would increase by ~50%, considering an increase of BC MAC from 7.5 (used in GEOS-Chem) to 11.3 m^2 g^{-1} as recommended by *Bond et al.* [2013].

In Figure 12, we further compare the spatial distributions of simulated annual mean all-sky TOA DRF of BC in China in 1980, 1990, and 2010. The three years are selected as surface concentrations (column burdens) of BC averaged over China are highest in 1990 (2010) but lowest in 1980 (Figure 7). The spatial distributions of TOA BC DRF are similar to those of surface BC concentrations (Figure 3), which are high in the regions with strong surface BC. The strongest values of BC DRF are about 3.1 W m^{-2} in 1980, 4.2 in 1990, and 4.6 in 2010. From 1980 to 1990 (2010), the DRF shows a significant increase of >0.3 (>0.5) W m^{-2} in the most region of eastern China, with the largest value of 1.1 (1.4) W m^{-2} in the Sichuan Basin.

We note that BC DRF in most regions of China is larger in 2010 than in 1990; in contrast, surface BC concentrations are lower in 2010 than in 1990. The discrepancy is largely because the column burdens of BC are higher in 2010 than in 1990 by 0.04 mg m^{-2} (4%) below 10 km and by 0.07 mg m^{-2} (18%) at 1–6 km (Figure 13a). Previous studies have shown that vertical distribution of BC is critical for the calculation of BC DRF [e.g., *Bond et al.*, 2013; *Li et al.*, 2016]. The BC DRF enhances considerably when BC is located at high altitude largely because of the radiative interactions with clouds [*Samset et al.*, 2013]. Relative to 1990, the higher BC concentrations above 1 km in 2010 thus largely account for the stronger DRF of BC in the year.

We find that column burdens of BC are higher in 2010 than in 1990 by 0.03 mg m^{-2} in VMET and by 0.01 mg m^{-2} in VEMIS. The corresponding values at 1–6 km are 0.04 mg m^{-2} in VMET and 0.03 mg m^{-2} in VEMIS. These sensitivity simulations indicate that meteorological parameters are an important factor that accounts for the different DRF between 2010 and 1990. Our companion study of Y. H. Mao et al. (to be submitted, 2016) showed that year 1990 is a relatively weaker monsoon year compared to year 2010 and therefore has a weaker vertical convection, which results in the significantly lower BC concentrations at 1–6 km (with the maximum of ~0.03 µg m^{-3}, Figure 13a).

In addition, the impact of non-China emissions is significant on vertical profiles and hence DRF of BC in China. *Li et al.* [2016], using the GEOS-Chem model, reported that percentage contributions of non-China emissions to BC concentrations generally increase with altitudes, and contribution at 5 km altitude is larger than 20% in China, especially high ($>80\%$) in northwestern China and the Tibetan plateau. The seasonal contributions of non-China emissions to BC DRF reach about 17–43% in China. We find that the percentage contributions of non-China emissions to column burden of BC are 18–27% below 10 km and 25–36% at 1–6 km (Figure 13b). The non-China emissions account for 0.32 W m^{-2} (31%) of simulated all-sky TOA DRF of BC averaged over China in 2010, with the largest values in southeastern China (~1.0 W m^{-2}, Figure 12). Relative to year 1990, the contribution of non-China emissions to column burden of BC is larger in 2010 by 0.04 mg m^{-2} below 10 km and by 0.03 mg m^{-2} at 1–6 km. The increasing contribution of non-China emissions to BC is thus another important factor leading to the higher BC DRF in 2010 than in 1990.

7. Summary and Conclusions

We examined the impacts of variations in meteorological parameters and emissions on the decadal and inter-annual variations of surface concentrations and tropospheric column burden of BC in China for 1980–2010
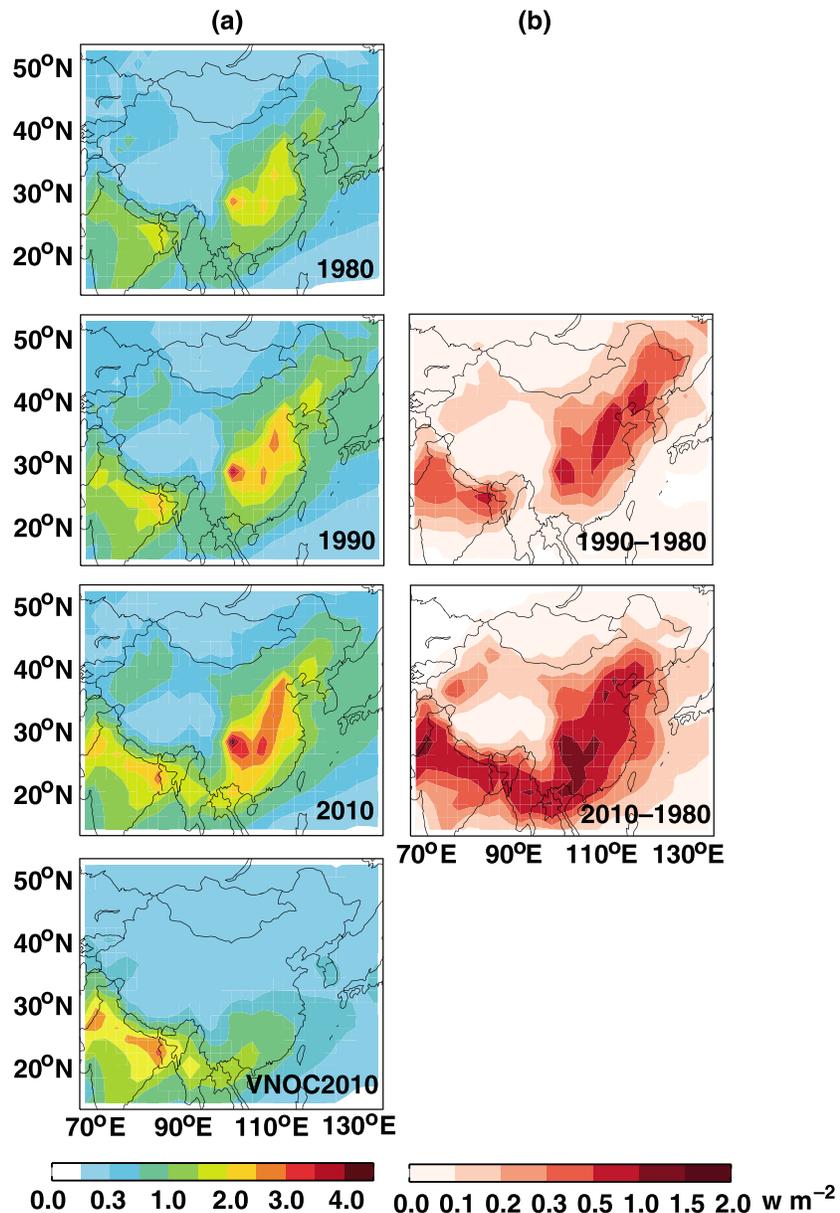
Figure 12. (a) Simulated annual mean all-sky direct radiative forcing (DRF) of BC (W m^{-2}) at the top of the atmosphere (TOA) in 1980 (the year of the lowest surface concentrations and tropospheric column burdens of BC averaged over China), 1990 (the year of the highest surface concentrations), and 2010 (the year of the highest tropospheric column burdens). Results are from model simulation VALL. Also shown are simulated annual mean all-sky TOA DRF of BC (W m^{-2}) in 2010 from model simulation VNOC. (b) Differences in simulated annual mean all-sky TOA DRF of BC (W m^{-2}) between 1990 and 1980 and between 2010 and 1980.

using the GEOS-Chem model driven by the MERRA meteorological fields. The impacts of variations in meteorological parameters and emissions on BC were imposed separately and together by sensitivity simulations.

Model results generally captured the decadal and interannual variations of BC in China for 1980–2010. Simulated annual mean BC surface concentrations and AAOD were generally biased low by −49% and −50%, respectively, compared with the corresponding observations at remote and rural sites. With doubled anthropogenic emissions of BC in Asia, simulated annual mean BC surface concentrations and AAOD were in fair agreement with observations at most of the remote and rural sites (with NMBs of 1% and 4%, respectively). The correlation coefficients were larger than 0.3 and 0.25, respectively, between simulated annual
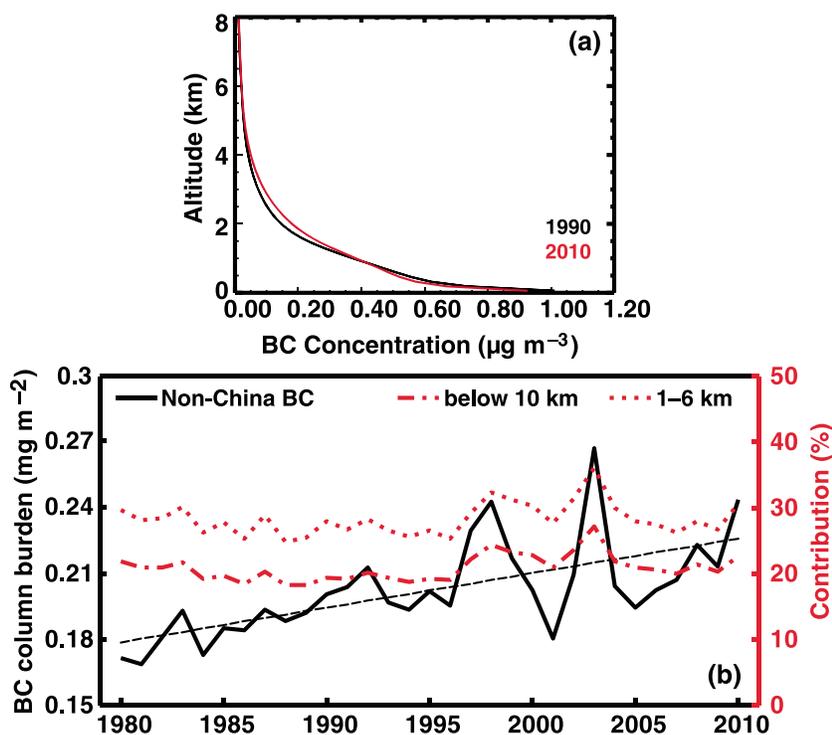
Figure 13. (a) Simulated vertical profiles of BC mass concentrations ($\mu g\, m^{-3}$) in 1990 (black) and in 2010 (red). Results are annual mean averages over China from model simulation VALL. (b) Contributions of non-China emissions to tropospheric column burdens of BC (left y axis, black solid, below 10 km, $mg\, m^{-2}$) averaged over China for 1980–2010 from model simulation VNOC. The black dotted line is linear regression using the least squares fit approach. Also shown are the percentage contributions (VNOC × 100%/VALL) below 10 km and at 1–6 km (right y axis, red, %).

mean BC concentrations in the atmosphere and observed annual BC concentrations in ice cores in the Tibetan Plateau and in lake sediments in eastern China.

Simulated surface BC concentrations were highest in eastern China and larger than $6\, \mu g\, m^{-3}$ in the densely populated and heavily industrialized areas. Relative to 1980, simulated surface BC concentrations in 2010 increased by $0.29\, \mu g\, m^{-3}$ (24%) averaged over eastern China and by $0.12\, \mu g\, m^{-3}$ (66%) over western China. The increasing rates of surface BC concentrations between 1990 and 1980 were comparable in western (37%) and eastern (39%) China, while the corresponding value between 2010 and 2000 was higher in western China than in eastern China (27% versus 16%). From 1980 to 2010, simulated annual mean all-sky TOA DRF of BC increased by $0.35\, W\, m^{-2}$ (51%) averaged over China. In 2010, the non-China emissions account for $0.32\, W\, m^{-2}$ (31%) of simulated all-sky TOA DRF of BC.

Simulated annual mean surface concentrations (column burdens) of BC averaged over China were in the range of ~0.7–$1.0\, \mu g\, m^{-3}$ (~0.8–$1.1\, mg\, m^{-2}$), considering variations in both meteorological parameters and emissions. The corresponding variations of simulated annual mean surface concentrations (column burdens) of BC averaged over China were -20% to 15% (-20% to 11%) for DM, $0.068\, \mu g\, m^{-3}$ ($0.069\, mg\, m^{-2}$) for MAD, and 7.7% (7.1%) for APDM. The associated decadal trends were $0.31\, \mu g\, m^{-3}\, decade^{-1}$ ($0.29\, mg\, m^{-2}\, decade^{-1}$) in the 1980s, -0.20 (-0.10) in the 1990s, and 0.16 (0.21) in the 2000s. The decadal trends of BC in China were similar to the variations of emissions in China, indicating that changes in emissions were the major driver of the decadal trends of BC.

The interannual variations of detrended surface concentrations (column burdens) of BC averaged over China were $0.014\, \mu g\, m^{-3}$ ($0.019\, mg\, m^{-2}$) for MAD and 2.0% (2.5%) for APDM. We also found that the interannual variations of BC in China were dependent on variations in both meteorological parameters and emissions. Meteorological parameters played a crucial role in winter or in the Tibetan Plateau and northeastern China. Process analyses identified that the variation in transport was the major meteorological factor to influence

the interannual variations of BC. Anthropogenic emissions alone accounted for ~90% (70%) of emission-induced interannual variations of surface concentrations (column burdens) of BC annually and 42% (28%) of those in MAM fire seasons. Biomass burning emissions became an important driving factor in MAM, especially in the regions close to the sources (e.g., the north and south tips of mainland China). The influences of non-China emissions on BC are also largest in MAM.

Understanding the separate effects of changes in meteorological parameters and emissions in the variations of BC in China plays important roles in guiding the effective mitigation actions. For future studies, the cooling effect of BC coemitted species (e.g., organic matter and sulfate) calls for systematical analysis in the net climate effect of black carbon-rich sources and the further implications of BC mitigation in China.

References

Allen, D. J., R. B. Rood, A. M. Thompson, and R. D. Hudson (1996a), Three-dimensional radon 222 calculations using assimilated metrological data and a convective mixing algorithm, *J. Geophys. Res.*, *101*, 6871–6881.

Allen, D. J., P. Kasibhatla, A. M. Thompson, R. B. Rood, B. G. Doddridge, K. E. Pickering, R. D. Hudson, and S.-J. Lin (1996b), Transport-induced interannual variability of carbon monoxide determined using a chemistry and transport model, *J. Geophys. Res.*, *101*, 28,655–28,669.

Arakawa, A., and W. H. Schubert (1974), Interaction of a cumulus cloud ensemble with the large-scale environment, Part I, *J. Atmos. Sci.*, *31*, 674–701.

Bey, I., D. J. Jacob, R. M. Yantosca, J. A. Logan, B. D. Field, A. M. Fiore, Q. Li, H. Y. Liu, L. J. Mickley, and M. G. Schultz (2001), Global modeling of tropospheric chemistry with assimilated meteorology: Model description and evaluation, *J. Geophys. Res.*, *106*(D19), 23,073–23,095, doi:10.1029/2001JD000807.

Bond, T. C., and R. W. Bergstrom (2006), Light absorption by carbonaceous particles: An investigative review, *Aerosol Sci. Technol.*, *40*, 27–67, doi:10.1080/02786820500421521.

Bond, T. C., D. G. Streets, K. F. Yarber, S. M. Nelson, J.-H. Woo, and Z. Klimont (2004), A technology-based global inventory of black and organic carbon emissions from combustion, *J. Geophys. Res.*, *109*, D14203, doi:10.1029/2003JD003697.

Bond, T. C., E. Bhardwaj, R. Dong, R. Jogani, S. Jung, C. Roden, D. G. Streets, and N. M. Trautmann (2007), Historical emissions of black and organic carbon aerosol from energy-related combustion, 1850–2000, *Global Biogeochem. Cycles*, *21*, GB2018, doi:10.1029/2006GB002840.

Bond, T. C., et al. (2013), Bounding the role of black carbon in the climate system: Scientific assessment, *J. Geophys. Res. Atmos.*, *118*, 5380–5552, doi:10.1002/jgrd.50171.

Cao, J. J., B. Q. Xu, J. Q. He, X. Q. Liu, Y. M. Han, G. H. Wang, and C. S. Zhu (2009), Concentrations, seasonal variations, and transport of carbonaceous aerosol at a remote Mountainous region in western China, *Atmos. Environ.*, *43*, 4444–4452, doi:10.1016/j.atmosenv.2009.06.023.

Chen, H. Z., D. Wu, B. T. Liao, H. Y. Li, and F. Li (2013), Compare of black carbon concentration variation between Dongguan and Maofengshan [in Chinese], *China Environ. Sci.*, *33*(4), 605–612.

Chin, M., P. Ginoux, S. Kinne, O. Torres, B. N. Holben, B. N. Duncan, R. V. Martin, J. A. Logan, A. Higurashi, and T. Nakajima (2002), Tropospheric aerosol optical thickness from the GOCART model and comparisons with satellite and Sun photometer measurements, *J. Atmos. Sci.*, *59*, 461–483.

Chow, J. C., J. G. Watson, L. W. A. Chen, W. P. Arnott, and H. Moosmuller (2004), Equivalence of elemental carbon by thermal/optical reflectance and transmittance with different temperature protocols, *Environ. Sci. Technol.*, *38*, 4414–4422.

Clarke, A. D., et al. (2004), Size distributions and mixtures of dust and black carbon aerosol in Asian outflow: Physiochemistry and optical properties, *J. Geophys. Res.*, *109*, D15S09, doi:10.1029/2003JD004378.

Cong, Z., S. Kang, S. Gao, Y. Zhang, Q. Li, and K. Kawamura (2013), Historical trends of atmospheric black carbon on Tibetan Plateau as reconstructed from a 150-year lake sediment record, *Environ. Sci. Technol.*, *47*(6), 2579–2586.

Cooke, W. F., C. Liousse, H. Cachier, and J. Feichter (1999), Construction of a 1° × 1° fossil fuel emission data set for carbonaceous aerosol and implementation and radiative impact in the ECHAM4 model, *J. Geophys. Res.*, *104*(D18), 22,137–22,162, doi:10.1029/1999JD900187.

Davidson, C. I., et al. (1993), Chemical constituents in the air and snow at Dye 3, Greenland: II. Analysis of episodes in April 1989, *Atmos. Environ.*, *27*(A), 2723–2738.

Dubovik, O., B. Holben, T. F. Eck, A. Smirnov, Y. J. Kaufman, M. D. King, D. Tanré, and I. Slutsker (2002), Variability of absorption and optical properties of key aerosol types observed in worldwide locations, *J. Atmos. Sci.*, *59*, 590–608.

Flanner, M. G., C. S. Zender, J. T. Randerson, and P. J. Rasch (2007), Present-day climate forcing and response from black carbon in snow, *J. Geophys. Res.*, *112*, D11202, doi:10.1029/2006JD008003.

Flanner, M. G., C. S. Zender, P. G. Hess, N. M. Mahowald, T. H. Painter, V. Ramanathan, and P. J. Rasch (2009), Springtime warming and reduced snow cover from carbonaceous particles, *Atmos. Chem. Phys.*, *9*, 2481–2497.

Fu, T. M., et al. (2012), Carbonaceous aerosols in China: Top-down constraints on primary sources and estimation of secondary contribution, *Atmos. Chem. Phys.*, *12*(5), 2725–2746, doi:10.5194/acp-12-2725-2012.

Gao, C., Q. Lin, S. Zhang, J. He, X. Lu, and G. Wang (2014), Historical trends of atmospheric black carbon on Sanjiang Plain as reconstructed from a 150-year peat record, *Sci. Rep.*, *4*, 5723, doi:10.1038/srep05723.

Granier, C., et al. (2011), Evolution of anthropogenic and biomass burning emissions of air pollutants at global and regional scales during the 1980–2010 period, *Clim. Change*, *109*(1–2), 163–190.

Hack, J. J. (1994), Parameterization of moist convection in the NCAR community climate model (CCM2), *J. Geophys. Res.*, *99*, 5551–5568.

Han, Y. M., Z. W. Han, J. J. Cao, J. C. Chow, J. G. Watson, Z. S. An, S. X. Liu, and R. J. Zhang (2008), Distribution and origin of carbonaceous aerosol over a rural high-mountain lake area, Northern China and its transport significance, *Atmos. Environ.*, *42*, 2405–2414, doi:10.1016/j.atmosenv.2007.12.020.

Han, Y. M., J. J. Cao, B. Z. Yan, T. C. Kenna, Z. D. Jin, Y. Cheng, J. C. Chow, and Z. S. An (2011), Comparison of elemental carbon in lake sediments measured by three different methods and 150-year pollution history in eastern China, *Environ. Sci. Technol.*, *45*, 5287–5293.

He, C., et al. (2014), A global 3-D CTM evaluation of black carbon in the Tibetan Plateau, *Atmos. Chem. Phys.*, *14*(13), 7091–7112, doi:10.5194/acp-14-7091-2014.

Heald, C. L., D. A. Ridley, J. H. Kroll, S. R. H. Barrett, K. E. Cady-Pereira, M. J. Alvarado, and C. D. Holmes (2014), Contrasting the direct radiative effect and direct radiative forcing of aerosols, *Atmos. Chem. Phys.*, *14*(11), 5513–5527, doi:10.5194/acp-14-5513-2014.

Holben, B. N., et al. (2001), An emerging ground-based aerosol climatology: Aerosol optical depth from AERONET, *J. Geophys. Res.*, *106*(D11), 12,067–12,097, doi:10.1029/2001JD900014.

Horvath, H. (1993), Atmospheric light absorption—A review, *Atmos. Environ.*, *27*, 293–317.

Intergovernmental Panel on Climate Change (IPCC) (2013), *Climate Change 2013: The Physical Science Basis. Contribution of Working Group I to the Fifth Assessment Report of the Intergovernmental Panel on Climate Change*, edited by T. F. Stocker et al., pp. 1535 , Cambridge Univ. Press, Cambridge, U. K., and New York.

Jacobson, M. Z. (2004), Climate response of fossil fuel and biofuel soot, accounting for soot's feedback to snow and sea ice albedo and emissivity, *J. Geophys. Res.*, *109*, D21201, doi:10.1029/2004JD004945.

Jacobson, M. Z. (2006), Effects of externally-through-internally-mixed soot inclusions within clouds and precipitation on global climate, *J. Phys. Chem. A*, *110*, 6860–6873, doi:10.1021/Jp056391r.

Jeong, J. I., and R. J. Park (2013), Effects of the meteorological variability on regional air quality in East Asia, *Atmos. Environ.*, *69*, 46–55, doi:10.1016/J.Atmosenv.2012.11.061.

Jeong, J. I., R. J. Park, J.-H. Woo, Y.-J. Han, and S.-M. Yi (2011), Source contributions to carbonaceous aerosol concentrations in Korea, *Atmos. Environ.*, *45*(5), 1116–1125, doi:10.1016/j.atmosenv.2010.11.031.

Junker, C., and C. Liousse (2008), A global emission inventory of carbonaceous aerosol from historic records of fossil fuel and biofuel consumption for the period 1860–1997, *Atmos. Chem. Phys.*, *8*, 1195–1207, doi:10.5194/acp-8-1195-2008.

Kaiser, J. W., et al. (2012), Biomass burning emissions estimated with a global fire assimilation system based on observed fire radiative power, *Biogeosciences*, *9*, 527–554, doi:10.5194/bg-9-527-2012.

Kopacz, M., D. L. Mauzerall, J. Wang, E. M. Leibensperger, D. K. Henze, and K. Singh (2011), Origin and radiative forcing of black carbon transported to the Himalayas and Tibetan Plateau, *Atmos. Chem. Phys.*, *11*(6), 2837–2852, doi:10.5194/acp-11-2837-2011.

Kurokawa, J., T. Ohara, T. Morikawa, S. Hanayama, G. Janssens-Maenhout, T. Fukui, K. Kawashima, and H. Akimoto (2013), Emissions of air pollutants and greenhouse gases over Asian regions during 2000–2008: Regional Emission inventory in ASia (REAS) version 2, *Atmos. Chem. Phys.*, *13*, 11,019–11,058, doi:10.5194/acp-13-11019-2013.

Li, K., H. Liao, Y. H. Mao, and D. A. Ridley (2016), Sectoral and Regional Contributions to Black Carbon and its Direct Radiative Forcing in China, *Atmos. Environ.*, *124*, 351–366, doi:10.1016/j.atmosenv.2015.06.014.

Lin, S.-J., and R. B. Rood (1996), Multidimensional flux-form semi-Lagrangian transport schemes, *Mon. Weather Rev.*, *124*, 2046–2070.

Liu, H., D. J. Jacob, I. Bey, and R. M. Yantosca (2001), Constraints from 210Pb and 7Be on wet deposition and transport in a global three-dimensional chemical tracer model driven by assimilated meteorological fields, *J. Geophys. Res.*, *106*(D11), 12,109–12,128, doi:10.1029/2000JD900839.

Lu, Z., Q. Zhang, and D. G. Streets (2011), Sulfur dioxide and primary carbonaceous aerosol emissions in China and India, 1996–2010, *Atmos. Chem. Phys.*, *11*(18), 9839–9864, doi:10.5194/acp-11-9839-2011.

Malm, W. C., J. F. Sisler, D. Huffman, R. A. Eldred, and T. A. Cahill (1994), Spatial and seasonal trends in particle concentration and optical extinction in the United States, *J. Geophys. Res.*, *99*, 1347–1370.

Mao, Y. H., Q. B. Li, L. Zhang, Y. Chen, J. T. Randerson, D. Chen, and K.-N. Liou (2011), Biomass burning contribution to black carbon in the Western United States Mountain Ranges, *Atmos. Chem. Phys.*, *11*, 11,253–11,266, doi:10.5194/acp-11-11253-2011.

Ming, J., H. Cachier, C. Xiao, D. Qin, S. Kang, S. Hou, and J. Xu (2008), Black carbon record based on a shallow Himalayan ice core and its climatic implications, *Atmos. Chem. Phys.*, *8*, 1343–1352, doi:10.5194/acp-8-1343-2008.

Ming, J., C. D. Xiao, J. Y. Sun, S. C. Kang, and P. Bonasoni (2010), Carbonaceous particles in the atmosphere and precipitation of the Nam Co region, central Tibet, *J. Environ. Sci.*, *22*, 1748–1756, doi:10.1016/S1001-0742(09)60315-6.

Moorthi, S., and M. J. Suarez (1992), Relaxed Arakawa-Schubert: A parameterization of moist convection for general circulation models, *Mon. Weather Rev.*, *120*, 978–1002.

Mu, Q., and H. Liao (2014), Simulation of the interannual variations of aerosols in China: Role of variations in meteorological parameters, *Atmos. Chem. Phys.*, *14*, 9597–9612, doi:10.5194/acp-14-9597-2014.

Novakov, T., V. Ramanathan, J. E. Hansen, T. W. Kirchstetter, M. Sato, J. E. Sinton, and J. A. Sathaye (2003), Large historical changes of fossil-fuel black carbon aerosols, *Geophys. Res. Lett.*, *30*(6, 1324), doi:10.1029/2002GL016345.

Ohara, T., H. Akimoto, J. Kurokawa, N. Horii, K. Yamaji, X. Yan, and T. Hayasaka (2007), An Asian emission inventory of anthropogenic emission sources for the period 1980–2020, *Atmos. Chem. Phys.*, *7*, 4419–4444.

Park, R. J., D. J. Jacob, M. Chin, and R. V. Martin (2003), Sources of carbonaceous aerosols over the United States and implications for natural visibility, *J. Geophys. Res.*, *108*(D12), 4355, doi:10.1029/2002JD003190.

Penner, J. E., M. J. Prather, I. S. Isaksen, J. S. Fuglestvedt, Z. Klimont, and D. S. Stevenson (2010), Short-lived uncertainty?, *Nat. Geosci.*, *3*(9), 587–588.

Qin, Y., and S. D. Xie (2012), Spatial and temporal variation of anthropogenic black carbon emissions in China for the period 1980–2009, *Atmos. Chem. Phys.*, *12*(11), 4825–4841, doi:10.5194/acp-12-4825-2012.

Qu, W. J., X. Y. Zhang, R. Arimoto, D. Wang, Y. Q. Wang, L. W. Yan, and Y. Li (2008), Chemical composition of the background aerosol at two sites in southwestern and northwestern China: Potential influences of regional transport, *Tellus*, *60B*, 657–673, doi:10.1111/j.1600-0889.2008.00342.x.

Ramanathan, V., and G. Carmichael (2008), Global and regional climate changes due to black carbon, *Nat. Geosci.*, *1*(4), 221–227, doi:10.1038/ngeo156.

Randerson, J. T., Y. Chen, G. R. van der Werf, B. M. Rogers, and D. C. Morton (2012), Global burned area and biomass burning emissions from small fires, *J. Geophys. Res.*, *117*, G04012, doi:10.1029/2012JG002128.

Reddy, M. S., O. Boucher, N. Bellouin, M. Schulz, Y. Balkanski, J. L. Dufresne, and M. Pham (2005), Estimates of global multicomponent aerosol optical depth and direct radiative perturbation in the Laboratoire de Meteorologie Dynamique general circulation model, *J. Geophys. Res.*, *110*, D10S16, doi:10.1029/2004JD004757.

Rienecker, M. M., et al. (2011), MERRA: NASA's Modern-Era Retrospective Analysis for Research and Applications, *J. Clim.*, *24*, 3624–3648, doi:10.1175/JCLI-D-11-00015.1.

Samset, B. H., et al. (2013), Black carbon vertical profiles strongly affect its radiative forcing uncertainty, *Atmos. Chem. Phys.*, *13*(5), 2423–2434, doi:10.5194/acp-13-2423-2013.

Schultz, M. G., A. Heil, J. J. Hoelzemann, A. Spessa, K. Thonicke, J. G. Goldammer, A. C. Held, J. M. C. Pereira, and M. van het Bolscher (2008), Global wildland fire emissions from 1960 to 2000, *Global Biogeochem. Cycles*, *22*, GB2002, doi:10.1029/2007GB003031.

Shindell, D., et al. (2012), Simultaneously mitigating near-term climate change and improving human health and food security, *Science*, *335*(6065), 183–189, doi:10.1126/science.1210026.

Smith, S. J., and A. Mizrahi (2013), Near-term climate mitigation by short-lived forcers, *Proc. Natl. Acad. Sci. U. S. A.*, *110*(35), 14,202–14,206, doi:10.1073/pnas.1308470110.

Streets, D. G., T. C. Bond, T. Lee, and C. Jang (2004), On the future of carbonaceous aerosol emissions, *J. Geophys. Res.*, *109*, D24212, doi:10.1029/2004JD004902.

Streets, D. G., Y. Wu, and M. Chin (2006), Two-decadal aerosol trends as a likely explanation of the global dimming/brightening transition, *Geophys. Res. Lett.*, *33*, L15806, doi:10.1029/2006GL026471.

Streets, D. G., C. Yu, Y. Wu, M. Chin, Z. Zhao, T. Hayasaka, and G. Shi (2008), Aerosol trends over China, 1980–2000, *Atmos. Res.*, *88*, 174–182.

Textor, C., et al. (2006), Analysis and quantification of the diversities of aerosol life cycles within AeroCom, *Atmos. Chem. Phys.*, *6*, 1777–1813, doi:10.5194/acp-6-1777-2006.

van der Werf, G. R., J. T. Randerson, L. Giglio, G. J. Collatz, P. S. Kasibhatla, and A. F. Arellano Jr. (2006), Interannual variability in global biomass burning emission from 1997 to 2004, *Atmos. Chem. Phys.*, *6*, 3423–3441.

van der Werf, G. R., J. T. Randerson, L. Giglio, G. J. Collatz, M. Mu, P. S. Kasibhatla, D. C. Morton, R. S. DeFries, Y. Jin, and T. T. van Leeuwen (2010), Global fire emissions and the contribution of deforestation, savanna, forest, agricultural, and peat fires (1997–2009), *Atmos. Chem. Phys.*, *10*(23), 11,707–11,735, doi:10.5194/acp-10-11707-2010.

Walcek, C. J., R. A. Brost, and J. S. Chang (1986), SO_2, sulfate and HNO_3 deposition velocities computed using regional land use and meteorological data, *Atmos. Environ.*, *20*, 949–964.

Wang, M., et al. (2014), Carbonaceous aerosols recorded in a Southeastern Tibetan glacier: Variations, sources and radiative forcing, *Atmos. Chem. Phys. Discuss.*, *14*, 19,719–19,746, doi:10.5194/acpd-14-19719-2014.

Wang, Q., et al. (2011), Sources of carbonaceous aerosols and deposited black carbon in the Arctic in winter-spring: Implications for radiative forcing, *Atmos. Chem. Phys.*, *11*(23), 12,453–12,473, doi:10.5194/acp-11-12453-2011.

Wang, Q., D. J. Jacob, J. R. Spackman, A. E. Perring, J. P. Schwarz, N. Moteki, E. A. Marais, C. Ge, J. Wang, and S. R. H. Barrett (2014), Global budget and radiative forcing of black carbon aerosol: Constraints from pole-to-pole (HIPPO) observations across the Pacific, *J. Geophys. Res. Atmos.*, *119*, 195–206, doi:10.1002/2013JD020824.

Wang, R., et al. (2012), Black carbon emissions in China from 1949 to 2050, *Environ. Sci. Technol.*, *46*(14), 7595–7603, doi:10.1021/es3003684.

Xu, B., et al. (2009), Black soot and the survival of Tibetan glaciers, *Proc. Natl. Acad. Sci. U. S. A.*, *106*(52), 22,114–22,118.

Yang, Y., H. Liao, and S. Lou (2015), Decadal trend and interannual variation of outflow of aerosols from East Asia: Roles of variations in meteorological parameters and emissions, *Atmos. Environ.*, *100*, 141–153.

Zhang, L., L. Zhang, D. Zhang, S. Zhao, J. Huang, W. Zhang, and J. Shi (2011), Property of black carbon concentration over outskirts of Lanzhou, Northwest China (in Chinese), *China Environ. Sci.*, *31*(8), 1248–1255.

Zhang, Q., et al. (2009), Asian emissions in 2006 for the NASA INTEX-B mission, *Atmos. Chem. Phys.*, *9*(14), 5131–5153, doi:10.5194/acp-9-5131-2009.

Zhang, X. Y., Y. Q. Wang, X. C. Zhang, W. Guo, and S. L. Gong (2008), Carbonaceous aerosol composition over various regions of China during 2006, *J. Geophys. Res.*, *113*, D14111, doi:10.1029/2007JD009525.

Zhang, X. Y., Y. Q. Wang, T. Niu, X. C. Zhang, S. L. Gong, Y. M. Zhang, and J. Y. Sun (2012), Atmospheric aerosol compositions in China: Spatial/temporal variability, chemical signature, regional haze distribution and comparisons with global aerosols, *Atmos. Chem. Phys.*, *12*, 779–799, doi:10.5194/acp-12-779-2012.

Zhao, Y., P. Liu, J. Wang, and B. Li (2014), Characteristics of atmospheric background chemical component at Mt. Waliguan for 1991–2011 (in Chinese), *J. Qinghai Environ.*, *24*(1), 32–35, doi:10.3969/j.issn.1007-2454.2014.01.006.

Zhu, J., H. Liao, and J. Li (2012), Increases in aerosol concentrations over eastern China due to the decadal-scale weakening of the East Asian summer monsoon, *Geophys. Res. Lett.*, *39*, L09809, doi:10.1029/2012GL051428.